npj | parkinson's disease

Article

Published in partnership with the Parkinson's Foundation

https://doi.org/10.1038/s41531-024-00851-7

Park7 deletion leads to sex-specific transcriptome changes involving NRF2-CYP1B1 axis in mouse midbrain astrocytes

Sergio Helgueta[1,2], Tony Heurtaux[1,2], Alessia Sciortino[2,3], Yujuan Gui[1], Jochen Ohnmacht[1,3,4], Pauline Mencke[3], Ibrahim Boussaad[3], Rashi Halder[3], Pierre Garcia[2,3], Rejko Krüger[3,4,5], Michel Mittelbronn[1,2,3,4,6], Manuel Buttini[2,3], Thomas Sauter[1] & Lasse Sinkkonen[1] ✉

Loss-of-function mutations in *PARK7*, encoding for DJ-1, can lead to early onset Parkinson's disease (PD). In mice, *Park7* deletion leads to dopaminergic deficits during aging, and increased sensitivity to oxidative stress. However, the severity of the reported phenotypes varies. To understand the early molecular changes upon loss of DJ-1, we performed transcriptomic profiling of midbrain sections from young mice. While at 3 months the transcriptomes of both male and female mice were unchanged compared to their wildtype littermates, an extensive deregulation was observed in 8 month-old males. The affected genes are involved in processes like focal adhesion, extracellular matrix interaction, and epithelial-to-mesenchymal transition (EMT), and enriched for primary target genes of NRF2. Consistently, the antioxidant response was altered specifically in the midbrain of male DJ-1 deficient mice. Many of the misregulated genes are known target genes of estrogen and retinoic acid signaling and show sex-specific expression in wildtype mice. Depletion of DJ-1 or NRF2 in male primary astrocytes recapitulated many of the in vivo changes, including downregulation of CYP1B1, an enzyme involved in estrogen and retinoic acid metabolism. Interestingly, knock-down of CYP1B1 led to gene expression changes in focal adhesion and EMT in primary male astrocytes. Finally, male iPSC-derived astrocytes with loss of function mutation in the *PARK7* gene also showed changes in the EMT pathway and NRF2 target genes. Taken together, our data indicate that loss of *Park7* leads to sex-specific gene expression changes through astrocytic alterations in the NRF2-CYP1B1 axis, suggesting higher sensitivity of males to loss of DJ-1.

The clinical diagnosis of Parkinson's disease (PD) relies on the presence of specific motor symptoms, although non-motor symptoms such as hyposmia, depression, anxiety, dementia, autonomic and cognitive dysfunction or REM sleep behavior disorder can be present up to 20 years prior to initial PD diagnosis[1,2]. PD has an increasing incidence in the population above the age of 65[3], while prevalence and incidence of PD are higher in males than in females[4,5]. One of the most characteristic neuropathological hallmarks of PD is the progressive loss of dopaminergic neurons in the substantia nigra pars compacta (SNpc of the midbrain) leading to striatal dopamine deficiency[6]. One of the main drivers of this loss is oxidative stress and subsequent mitochondrial dysfunction, resulting in increased levels of reactive oxygen species (ROS)[7–9]. Neurons depend on glial cells such as microglia, oligodendrocytes, and astrocytes for their protection against oxidative stress. The accumulation of ROS in all these cell types is sensed by NRF2 pathway through oxidation of Kelch-like ECH-associated protein 1 (KEAP1) that leads to release and stabilization of Nuclear factor erythroid 2-related

[1]Department of Life Sciences and Medicine (DLSM), University of Luxembourg, Belvaux, Luxembourg. [2]Luxembourg Centre of Neuropathology (LCNP), Luxembourg, Luxembourg. [3]Luxembourg Centre for Systems Biomedicine (LCSB), University of Luxembourg, Belvaux, Luxembourg. [4]Luxembourg Institute of Health (LIH), Luxembourg, Luxembourg. [5]Centre Hospitalier de Luxembourg (CHL), Luxembourg, Luxembourg. [6]National Center of Pathology (NCP), Laboratoire National de Santé (LNS), Dudelange, Luxembourg. ✉e-mail: lasse.sinkkonen@uni.lu

factor 2 (NFE2L2, also known as NRF2), and its nuclear translocation, thereby inducing the expression of antioxidant response genes. A failure in antioxidant response can lead to oxidative stress[10]. Interestingly, the antioxidant response can be modulated by developmental signaling pathways and sexual hormones such as retinoic acid and estrogen, respectively, leading to differences in response depending on the cell state or sex[11]. In particular estrogen is associated with neuroprotection, possibly due to improved antioxidant response, and could contribute to sexual dimorphism of disease-risk in many disorders, including PD[12,13].

DJ-1 (encoded by *Parkinsonism associated deglycase* or *PARK7*) has been characterized as a causative gene for autosomal recessive, early onset PD[14] and the PD-associated mutations in the gene are typically leading to loss or reduction of the functional DJ-1 protein[15]. To date, various functions have been reported for DJ-1, mostly associated with mitochondrial biology and oxidative stress[16]. In both mouse and human cell lines, DJ-1 was shown to stabilize NRF2 through inhibition of its interaction with KEAP1[17]. Different primary mouse cell and animal models have been utilized to investigate the consequences of *Park7* gene disruption. However, the literature shows inconsistent results with respect to *Park7*$^{-/-}$ mouse models for studying PD. Most of the studies show no dopaminergic neurodegeneration in the SNpc[18–22]. In addition, Pham and colleagues show that these mice have less dopaminergic neurons in the VTA and exhibit non-motor symptoms associated with early phases of PD, such as impairment in motivated behavior and cognition[22]. Goldberg et al. reported abnormal nigral dopaminergic physiology in *Park7*$^{-/-}$ mice, including altered excitability and firing of dopamine neurons projecting to the striatum, together with defects in locomotor activity[18]. In contrast to these studies, Rousseaux and colleagues report that their *Park7*$^{-/-}$ mouse model show early onset progressive dopaminergic cell loss, advancing from unilateral to bilateral with aging[23]. The authors also see degeneration at the locus coeruleus and mild motor behavior deficits at later time points[23]. Taken together, controversy still exists regarding the dopaminergic system phenotype exhibited by *Park7*$^{-/-}$ mice, with notable variations across studies. It is worth noting that some previous studies did not specify the sex of the used animals, which is a critical variable that could influence the observed phenotypes in this mouse model.

Here, we investigated the early gene expression changes in the midbrain of both male and female *Park7*$^{-/-}$ mice to obtain insights into the early events triggered by absence of DJ-1 in vivo and to investigate the possible sex-specific differences. Moreover, we performed cell type-specific investigation of *Park7*-depletion in cultured primary astrocytes through RNAi experiments, and confirmed the disease-relevance of our findings using human iPSC-derived astrocytes carrying a *PARK7* mutation. Together our results identify many changes specifically in the male midbrain with processes such as EMT and focal adhesion becoming altered in astrocytes in an NRF2-dependent manner. These findings could have implications on understanding of the mechanisms of DJ-1-associated PD and the higher PD-risk of males, and help to reconcile discrepant results regarding different *Park7*$^{-/-}$-mouse models.

Results

Park7 deletion induces transcriptomic changes specifically in midbrain of 8-month-old males

To identify the early gene expression changes induced by loss of DJ-1 in ventral midbrain in both males and females, we dissected midbrains from 3- and 8-month-old *Park7*$^{-/-}$ and wildtype littermate control mice and isolated total RNA for RNA sequencing (RNA-seq) (Fig. 1). Interestingly, only 3 and 7 differentially expressed genes (DEGs, FDR < 0.05) were identified in females and males, respectively, at the age of 3 months (Fig. 1b, c, Supplementary Table 1–2). In contrast, by 8 months the number of DEGs in females increased to 101 (Fig. 1d) and in males over 1200 DEGs with generally stronger fold changes were detected (Supplementary Table 1-2). To confirm the extensive changes observed in males, we collected additional midbrain samples for RNA-seq analysis from an independent cohort of mice, with many of the gene expression changes remaining (Supplementary Table 1–2). After combining the independent cohorts and applying a batch correction, 746 mostly downregulated DEGs were confirmed in males (Fig. 1e, Supplementary Table 1). Strikingly, only 8 of the 746 DEGs in males were shared with the 101 DEGs identified in females at the same age. Finally, to confirm that the lack of changes in 8 month-old females is not due to technical or biological variation between the female samples, for example due to estrus cycle, we analyzed the per-gene dispersions to estimate the median dispersion of each sample set (Supplementary Fig. 1). Interestingly, the second cohort of 8-month-old male samples showed increased dispersion compared to other sample sets, partially explaining the lower number of DEGs compared to the first cohort. However, importantly, the median dispersion in 8 month old females was not higher compared males. Thus, our results indicate that loss of DJ-1 leads to sex-specific gene expression changes in the midbrain, with males particularly affected.

Loss of DJ-1 in male mice downregulates genes involved in epithelial to mesenchymal transition, focal adhesion, and extracellular matrix composition

To better understand the male-specific gene regulatory changes, we performed enrichment analysis for the identified 746 DEGs. Focal adhesion was found to be the most enriched pathway in KEGG and WikiPathways databases and also among the top 5 GO cellular components (Fig. 2a–d, Supplementary Table 3). Consistently, extracellular matrix (ECM)-receptor interaction and regulation of ECM were found among the top pathways, indicating changes in cellular adhesion and integrin-mediated interaction with ECM in the *Park7*$^{-/-}$ mice. Other top pathways included PI3K-Akt signaling pathway, interferon gamma response, and early estrogen response. Finally, the process with most significant enrichment across the different databases was found to be epithelial mesenchymal transition (EMT) in the MSigDB Hallmark database (Fig. 2c). Enrichment analysis for the 101 DEGs obtained for 8-month-old females did not show any of the enriched pathways from males (Supplementary Fig. 2a–d, Supplementary Table 4). The 58 significantly differentially expressed genes associated with EMT were almost all downregulated in male *Park7*$^{-/-}$ mice (Fig. 2e). Consistently, *Cdh1*, encoding for E-cadherin, a well established marker of EMT[24], was the gene with strongest fold change across all of the DEGs (Fig. 2f, Supplementary Table 1). *Twist1*, encoding for a transcriptional regulator typically induced in EMT, was also among the strongly downregulated genes, indicating that the cells are not undergoing classical EMT but rather an EMT-like process involving many of the same genes. Importantly, the downregulation of *Cdh1* was confirmed by real time quantitative PCR (RT-qPCR) and by RNAscope to take place in midbrain of 8 month-old males, but was not observed in females or in isolated cortex from the same male mice (Fig. 2g, h, Supplementary Fig. 3a, b).

Sex-specific changes in *Park7*$^{-/-}$ mice are associated with lowered NRF2 signaling

Next we asked how the loss of DJ-1 can lead to the observed transcriptional changes and what are the transcription factors (TFs) involved. To address this, we took advantage of the existing public data on TF target genes identified through chromatin immunoprecipitation (ChIP) experiments and derived from the ENCODE project and ChIP Enrichment Analysis (ChEA) database[25]. When focusing on bona fide TFs, the strongest enrichment among the male, but not female, DEGs was found for the primary targets of NRF2 (encoded by *Nfe2l2* gene) (Fig. 3a) (Supplementary Fig. 2e). These consisted of over 70 DEGs that are known primary NRF2 targets, most of which were downregulated and found to be associated with EMT process (Fig. 3b). However, some known NRF2 target genes involved in reactive oxygen species (ROS) production were also found to be upregulated. These results indicate that NRF2 could be mediating the DJ-1 induced transcriptional changes, involving an overall decrease in NRF2-mediated signaling and antioxidant response. Indeed, analysis of well established antioxidant response genes confirmed their downregulation in *Park7*$^{-/-}$ mice (Fig. 3c). *Nfe2l2* itself also showed a trend of downregulation but was not found to be significant after multiple testing correction (FDR = 0.144). Importantly, for representative antioxidant response genes

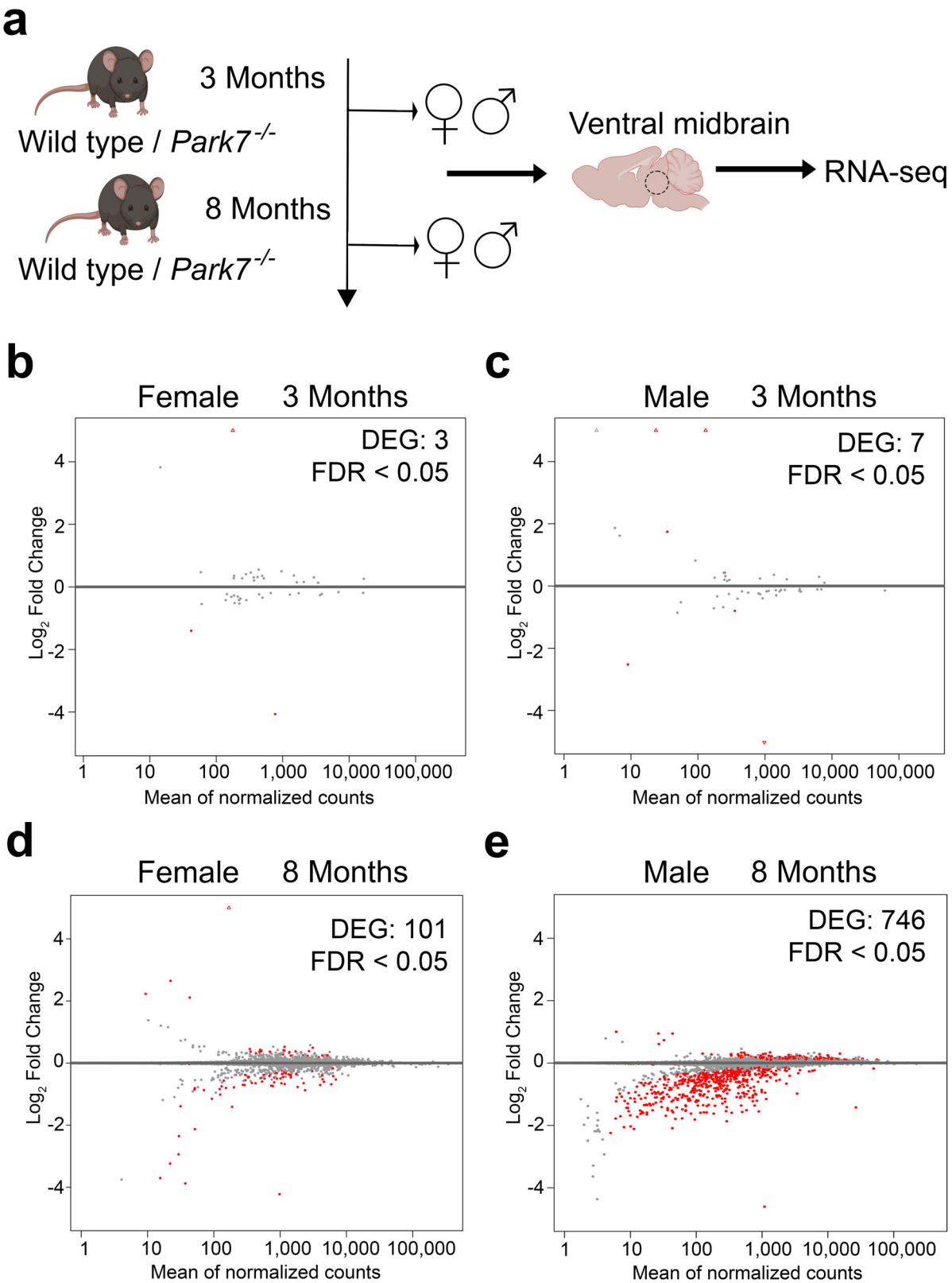

Fig. 1 | *Park7* deletion induces transcriptome deregulation during ageing predominantly in male ventral midbrain. a Schematic diagram of the experimental set-up for genome-wide transcriptomics profiling of isolated midbrains of 3-month-old and 8 month-old wild type and *Park7*$^{-/-}$ mice. **b**–**d** MA plots showing DEGs in the midbrains of *Park7*$^{-/-}$ mice compared to wildtype littermate controls in four different age- and sex-groups, namely (**b**) 3 month-old females (3 DEGs, $n = 4$), (**c**) 3 month-old males (7 DEGs, $n = 4$), (**d**) 8-month-old females (101 DEGs, $n = 4$), and (**e**) 8 month-old males (746 DEGs, $n = 8$). Each red dot represents one DEG defined by FDR < 0.05. The *x*-axis represents the mean of normalized counts and the *y*-axis the $\log_2$-fold change. Panel (**a**) was created with Biorender.com. Full lists of DEGs are available in Supplementary Table S1.

Gpx8, *Gstm2*, and *Ephx1*, the downregulation in male midbrain was again confirmed by RT-qPCR and found to be absent or modest in females or in cortex of the same males (Fig. 3d–g). Among upregulated genes, induction of *Irs2*, but not *Crim1*, was similarly confimed by RT-qPCR to occur in male midbrain (Supplementary Fig. 3c, d). Interestingly, by RT-qPCR also the downregulation of *Nfe2l2* was found to be significant in male midbrain (Fig. 3d), consistent with the known autoregulation of *Nfe2l2* locus by NRF2[26]. The lowered NRF2 activity was further confirmed by reduced signal for well-established NRF2-target gene *Gstm2* in RNAscope analysis of male midbrain sections from *Park7*$^{-/-}$ mice (Fig. 3h). No change in RNAscope signal could be observed in sections from female midbrain or male cortex (Supplementary Fig. 3e, f).

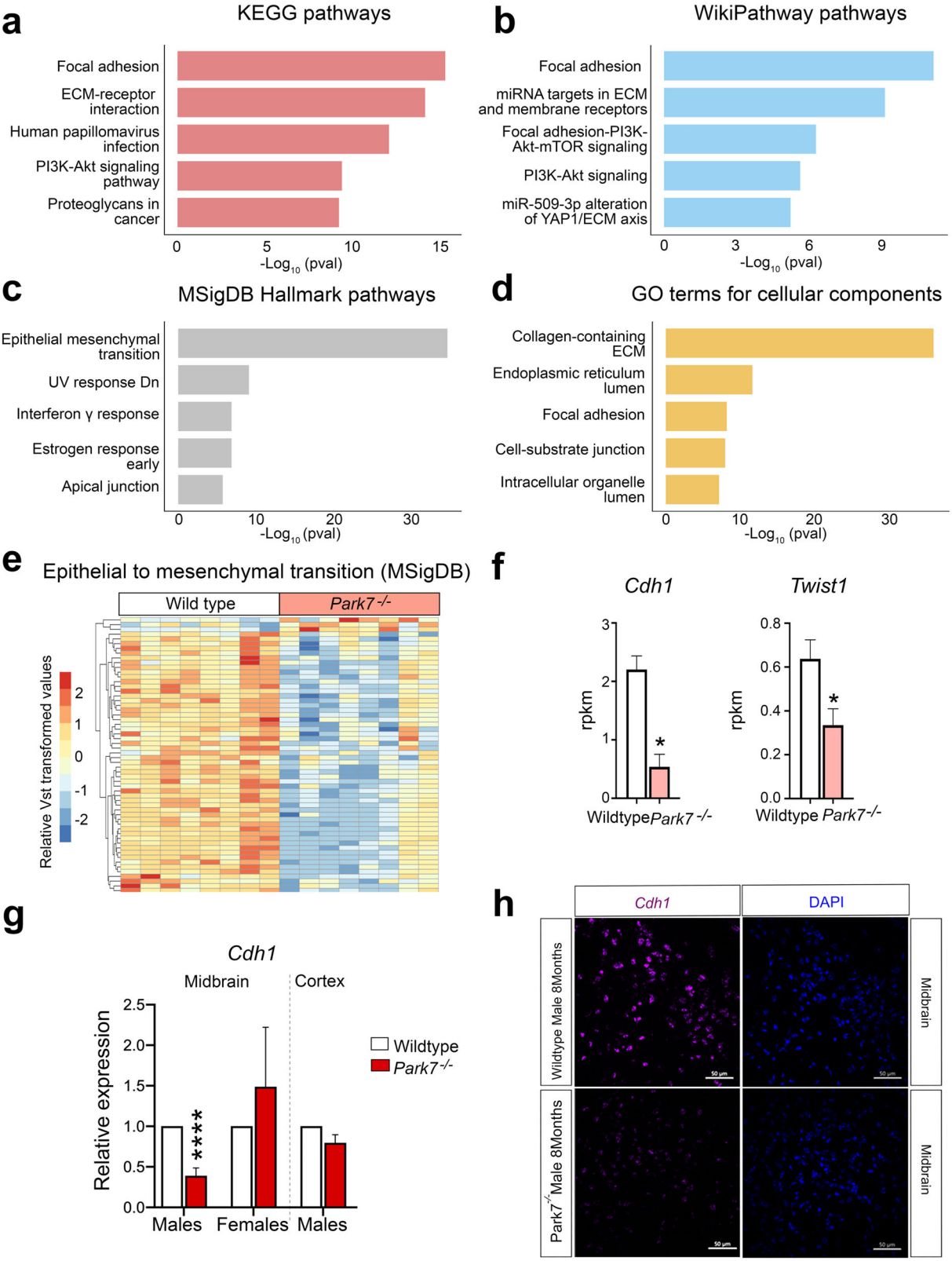

Fig. 2 | Loss of *Park7* alters expression of genes involved in focal adhesion, epithelial-to-mesenchymal transition, and extracellular matrix composition only in midbrain. a–d Pathway enrichment analysis for the 746 DEGs altered in 8-month-old male mice. The top 5 results from (**a**) KEGG pathways, (**b**) WikiPathway pathways, (**c**) MSigDB Hallmark pathways, and (**d**) GO terms for cellular components based on the significance of enrichment are shown.The *x*-axis represents the -$\log_{10}$ *p*-value of pathway enrichment. Complete results of enrichment analysis are available in the Supplementary Table S2. **e** Heatmap showing the relative expression of the 58 genes associated with EMT and found to be differentially expressed in midbrains of male *Park7*$^{-/-}$ mice compared to wild type littermates at 8-months of age. Vst-transformed read counts are plotted with each row representing one gene and each column representing an independent midbrain sample. **f** Expression levels in RPKM obtained by RNA-seq showing significant downregulation in the expression of *Cdh1* and *Twist1* in the midbrain of *Park7*$^{-/-}$ male mice at 8 months of age in comparison to wild type mice. *FDR < 0.05. **g** RT-qPCR validation of *Cdh1* downregulation in the midbrain of *Park7*$^{-/-}$ male mice at 8-months of age. No downregulation was observed in female midbrain or in male cortex. Values represent mean ± standard error of mean (SEM) (n = 4–8 mice per group). Statistical significance was tested by unpaired *t*-test. ****p-value < 0.0001. **h** RNAscope validation of *Cdh1* downregulation in the midbrain of *Park7*$^{-/-}$ male mice at 8 months of age. *Cdh1* mRNA is stained in purple, DAPI staining of DNA is in blue. Scale bar indicates 50 µm. Results for female midbrain and male cortex are available in Supplementary Fig. 3. Representative images from analysis of 3 independent mice per genotype are shown.

Genes altered by *Park7* deletion show sex-specific expression

To extend the analysis of the upstream events beyond direct TF binding, we performed upstream regulator prediction using Ingenuity Pathway Analysis (IPA) tool. Interestingly, the top upstream regulator predicted to explain most of expression changes in males was beta-estradiol, also known as *17β*-oestradiol, a key sex hormone and agonist for TFs called estrogen receptors (ERs) (Fig. 4a)[27]. This was not observed for females (Supplementary Fig. 2f). The top 5 regulators of male DEGs also included TGFβ, Agt, lipopolysaccharide, and tretinoin, also known as *all-trans* retinoic acid, an agonist of retinoic acid receptors (RARs). ERs and RARs have been described to exert opposing effects on their shared target genes through genomic antagonism[28], while both pathways are also known to influence NRF2 signaling[10].

Since the midbrain gene expression changes upon DJ-1 depletion are exhibiting sexual dimorphism, and oestradiol was recently described to control sex differences in the brain[29], we set out to identify the sexually dimorphic genes in the mouse midbrain at baseline. Differential gene expression analysis of the 8-month-old wildtype male and female midbrains identified 2516 DEGs between the sexes (Fig. 4b). Comparison of these genes with those misregulated in *Park7*$^{-/-}$ male mice showed an extensive and significant overlap, indicating that a large proportion of genes affected by loss of DJ-1 are also differentially expressed between males and females at baseline (Fig. 4c). Indeed, comparison of the fold changes of the overlapping genes in the different comparisons revealed a negative correlation, suggesting that genes with normally higher expression in males are reduced in expression in *Park7*$^{-/-}$ male mice (Fig. 4d).

To investigate this observation as a function of aging, we compared the DEG's expression changes between 3 and 8 months for each strain and sex. Strikingly, while the affected genes showed very few changes during aging in female mice or in *Park7*$^{-/-}$ males, a strong induction in expression could be observed for wildtype male mice (Fig. 4e). Suggesting that in wildtype males a sex-specifc expression increase occurs during aging for genes involved in processes such as anti-oxidant response. And this increase is not observed in absence of DJ-1.

DJ-1-NRF2-CYP1B1 axis regulates *Cdh1* expression in mouse astrocytes

Among the genes with higher expression in males and significant reduction in *Park7*$^{-/-}$ mice, we identified *Cyp1b1*, encoding a cytochrome P450 family enzyme that is involved in the metabolism of both *17β*-oestradiol and *all-trans* retinoic acid (Fig. 5)[30,31]. Recently, many P450 family enzymes, including *CYP1B1*, have been genetically associated with PD risk[32,33]. *Cyp1b1* was downregulated around 2-fold in the male midbrain as measured by RNA-seq and, similarly to other NRF2 target genes[34], this downregulation was confirmed by both RT-qPCR and RNAscope to take place in male midbrain but not in females or in male cortex (Fig. 5a-d, Supplementary Fig. 4a-b). The expression level of *Cyp1b1* in the midbrain samples was relatively low (~1 reads per kilo per million (RPKM)), suggesting that *Cyp1b1* might be selectively expressed in only some of the cell types of the brain. Indeed, analysis of Brain RNA-seq database[35] for purified cell types from mouse brain confirmed *Cyp1b1* to be mostly expressed in mouse astrocytes (Fig. 5c). Consistently, co-staining *Cyp1b1* by RNAscope and astrocytic marker GFAP by immunohistochemistry confirmed a common co-localization of the two signals in the midbrain (Fig. 5e). To further investigate the expression of CYP1B1 in astrocytes at protein level, we conducted parallel immunohistochemistry with antibodies against CYP1B1 and GFAP. The specificity of CYP1B1 antibody was confirmed by staining sections of kidney as positive control tissue (Supplementary Fig. 4c). Importantly, also antibody stainings of CYP1B1 often co-localized with GFAP signal, confirming CYP1B1 expression in midbrain astrocytes (Fig. 5f). However, not all CYP1B1 staining originated from GFAP-positive astrocytes, in keeping with the RNA-seq data (Fig. 5c). Finally, comparison of *Park7*$^{+/+}$ and *Park7*$^{-/-}$ mice indicated reduced CYP1B1 staining in the *Park7*-depleted males (Fig. 5f).

To analyse the possible contribution of *Cyp1b1* downregulation to the observed expression changes of genes involved in processes such as EMT, we isolated primary astrocytes separately from newborn male and female mice for RNA interference (RNAi) experiments (Fig. 6a). In parallel, microglia and oligodendrocyte precursors were also isolated as additional cell types with highly active NRF2 pathway but with lower *Cyp1b1* expression. The identities of the isolated cells were confirmed by stainings for markers of astrocytes (GFAP), microglia (F4/80), and oligodendrocytes (MBP) (Fig. 6b), and the sex of the mice was confirmed by PCR genotyping using *Ube* primers (Supplementary Fig. 5). To further control the purity of the primary cultures, transcriptomic analysis by RNA-seq was performed and used to inspect the expression of cell type-specific marker genes (Supplementary Fig. 6a). Moreover, we investigated the expression levels of different marker genes of reactive astrocyte to confirm that our culture conditions do not induce their activation (Supplementary Fig. 6b). Following the transfection of siRNAs targeting *Park7* mRNA, a strong downregulation of *Park7* was observed in all three cell types (Fig. 6c). Interestingly, this led to a significant downregulation of *Nfe2l2*, *Cyp1b1*, and the EMT-marker *Cdh1* in male astrocytes, but not in microglia and only for *Cyp1b1* in oligodendrocytes. Moreover, a downregulation of *Cdh1* was also observed in female astrocytes while an unexpected upregulation was detected in female microglia. To test whether the effect on *Cdh1* was mediated via NRF2 signaling, we also performed an *Nfe2l2* knock-down (Fig. 6d). Consistently, *Cyp1b1* and *Cdh1* were downregulated in male astrocytes, and for *Cyp1b1* also in female astrocytes, while microglia and oligodendrocytes remained largely unaffected. Finally, to test whether the misregulation of *Cyp1b1* could contribute to changes in *Cdh1* expression, we transfected oligodendrocytes, microglia and astrocytes with siRNAs targeting *Cyp1b1* and evaluated the expression of genes along the DJ-1-NRF2-CYP1B1 axis. While *Park7* and *Nfe2l2* were not reduced by *Cyp1b1* depletion, confirming their function upstream of *Cyp1b1*, *Cdh1* was significantly downregulated, especially in male astrocytes (Fig. 6e). Thus, the EMT pathway alterations in the midbrain of *Park7*$^{-/-}$ male mice are likely to take place in astrocytes and involve the NRF2-CYP1B1 axis.

Park7 deletion induced changes in focal adhesion and epithelial to mesenchymal transition involve NRF2 and CYP1B1 in astrocytes

To evaluate the genome-wide impact of the different knock-downs, we performed transcriptome analysis of the male astrocytes 24 h post-

transfection and compared to cells similarly treated with an unspecific control siRNA. Knock-down of *Park7*, *Nfe2l2*, and *Cyp1b1* induced a significant differential expression (FDR < 0.05) of 673, 1055, and 918 genes, respectively, when performing paired analysis (Fig. 7a–c, Supplementary Table 5). Also in primary astrocytes, more down- than upregulated genes were observed for each knock-down. Many of the DEGs were different from those detected in isolated midbrain, which could reflect the regional differences of astrocyte subpopulations from midbrain compared to astrocytes isolated from whole brain as was done here. Alternatively, this could also reflect the limitations of cell culture systems in mimicking the adult brain in the absence of the appropriate microenvironment. Interestingly, the upregulated genes were enriched for pathways such as interferon signaling and

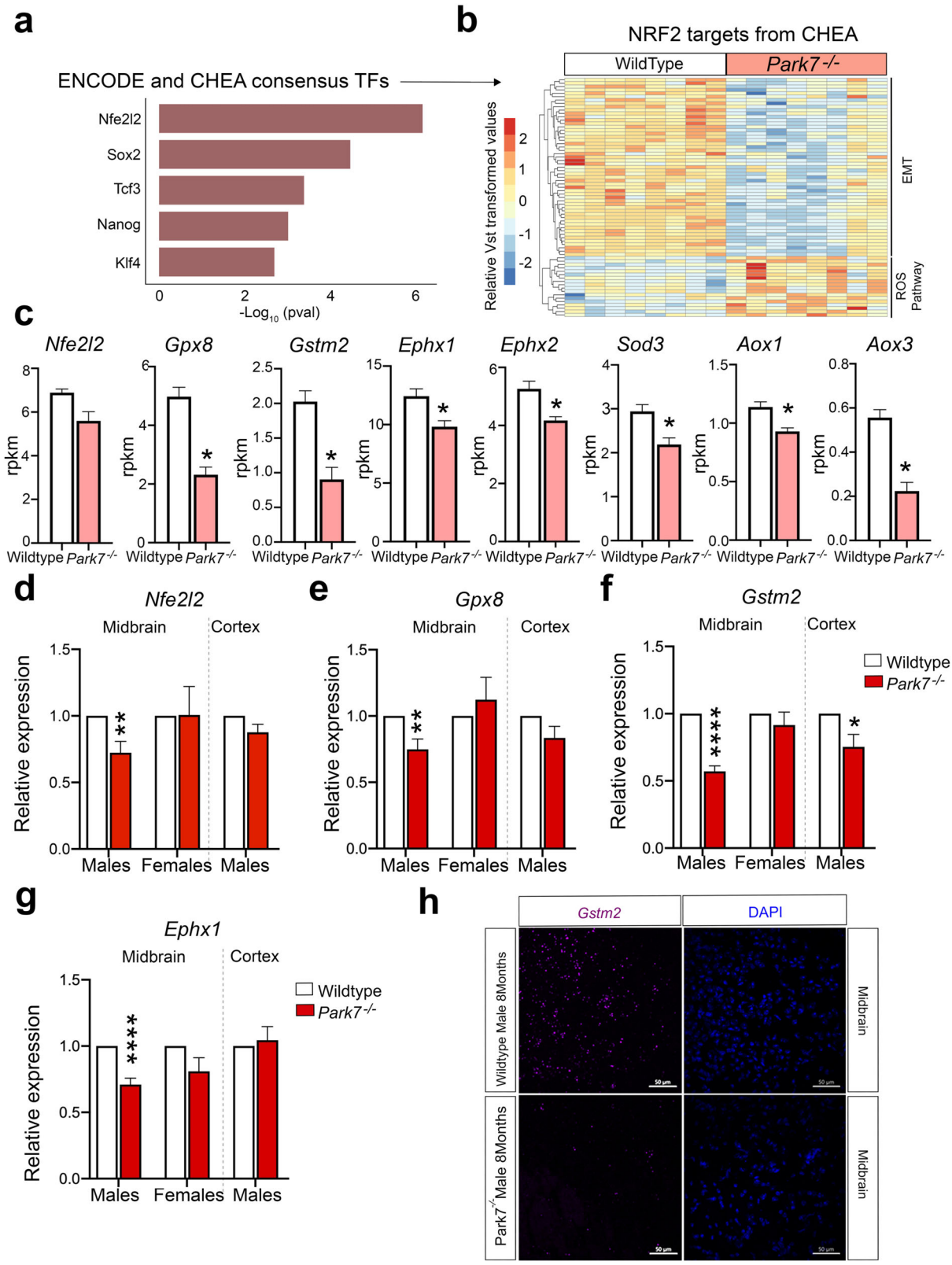

Fig. 3 | *Park7* depletion leads to reduced antioxidant response in mouse midbrain. a Top 5 TFs associated with DEGs from *Park7*$^{-/-}$ male mice based on the significance of enrichment for primary TF targets from the ENCODE project and ChEA database. NRF2, encoded by *Nfe2l2* gene, is the most enriched TF. The *x*-axis represents the -$\log_{10}$ *p*-value. **b** Heatmap showing the relative expression of the 70 primary NRF2 target genes from CHEA database found to be differentially expressed in midbrains of male *Park7*$^{-/-}$ mice compared to wild type littermates at 8 months of age. Vst-transformed read counts are plotted with each row representing one gene and each column representing an independent midbrain sample. **c** Expression levels in RPKM obtained by RNA-seq showing significant downregulation in the expression of several antioxidant response genes in the midbrain of *Park7*$^{-/-}$ male mice at 8 months of age in comparison to wild type mice. *FDR < 0.05. **d**–**g** RT-qPCR validation of (**d**) *Nfe2l2*, (**e**) *Gpx8*, (**f**) *Gstm2*, and (**g**) *Ephx1* downregulation in the midbrain of *Park7*$^{-/-}$ male mice at 8 monts of age. No downregulation was observed in female midbrain or in male cortex except for *Gstm2*. Values represent mean ± SEM (n = 4–8 mice per group). Statistical significance was tested by unpaired *t*-test. *p-value < 0.05; **p-value < 0.01; ****p-value < 0.0001. **h** RNAscope validation of *Gstm2* downregulation in the midbrain of *Park7*$^{-/-}$ male mice at 8 months of age. *Gstm2* mRNA is stained in purple, DAPI staining of DNA is in blue. Scale bar indicates 50 µm. Results for female midbrain and male cortex are available in Supplementary Fig. 3. Representative images from analysis of 3 independent mice per genotype are shown.

primary targets of IRF8 (Supplementary Fig. 7). However, when focusing on the top 5 pathway enrichments for downregulated genes upon *Park7* depletion in MSigDB Hallmark and WikiPathways databases, EMT and focal adhesion were among the top enriched pathways also in cultured astrocytes (Fig. 7d, e). When analysing the enrichments of the same top 5 pathways among the genes downregulated upon *Nfe2l2* or *Cyp1b1* depletion, it was clear that many of the pathways altered by *Park7* depletion, such as PI3K-Akt and interferon signaling, were not similarly affected (Fig. 7e and Supplementary Fig. 7). But importantly, both EMT and focal adhesion were significantly enriched also in these conditions. Suggesting that *Park7* deletion induced gene expression changes affecting EMT and focal adhesion are occurring in astrocytes and are mediated by NRF2 and CYP1B1. In keeping with this result, the downregulated genes for each knock-down in astrocytes were enriched for primary target genes of NRF2 (Fig. 7f).

Finally, we asked whether our findings in mouse astrocytes are also of relevance for human cellular models of PD. For this we took advantage of recent transcriptomic data of male iPSC-derived astrocytes with *PARK7* mutation (c.192 G > C) causing DJ-1 deficiency[15,36]. In the human astrocytes, 291 genes were significantly differentially expressed (FDR < 0.05) with 179 of those genes downregulated upon loss of DJ-1 (Fig. 8a). Albeit the number of available genes for enrichment analysis was limited, also in human astrocytes the most enriched pathways were EMT and interferon signaling for down- and upregulated genes, respectively (Fig. 8b-c). Suggesting that many of the male-specific changes upon DJ-1 depletion in mouse could also be relevant for PD diagnosis and disease progression in humans.

Discussion

Here, we have characterized the early transcriptome changes occuring in the midbrain of *Park7*$^{-/-}$ mice during aging. We report alterations specifically in the male midbrain, in keeping with the epidemiological data on higher PD prevalence in males[37]. Moreover, many of the transcriptional changes observed in males are affecting genes with sex-specific expression. Consistently, a homozygous female carrier of the c.192 G > C mutation of *PARK7* found in our human iPSC line was reported to be clinically asymptomatic at an age when a male patient was already affected[38]. The gene expression changes in the midbrain of male *Park7*$^{-/-}$ mice at 8 months of age were consistent with a downregulation of antioxidant response and reduction in the expression and activity of NRF2. Interestingly, expression of *NFE2L2* and NRF2 target genes have been reported to be decreased in the midbrain of PD patients[39] and DJ-1 is known to be involved in the stabilization and activation of NRF2[17]. In *Park7*$^{-/-}$ mice, the disruption of DJ-1 function alone might be sufficient to increase reactive oxygen species (ROS) production, but with the parallel decrease in the activity of NRF2 and the transcription of antioxidant genes, the accumulation of ROS is likely to lead to oxidative stress, one of the main hallmarks of PD[7–9]. Interestingly, these changes seem to take place selectively in the midbrain as no alterations were detected in the cortical tissues of the same male mice, in keeping with midbrain being the most affected area in PD[6,40].

It is unclear how the DJ-1-NRF2 interaction occurs. However, it is known that DJ-1 is able to activate PI3K-Akt and ERK pathways to exerts its cytoprotective role in an oxidative stress-associated neurotoxic context model of PD[41]. Moreover, PI3K-Akt pathway can activate NRF2 signaling[42,43] and was found enriched among DEGs in *Park7*$^{-/-}$ mice and upon *Park7* knockdown in primary astrocytes. Therefore, in the absence of DJ-1, PI3K-Akt signaling may be reduced (possibly through the inhibition of PTEN[44,45]), leading to a decreased stabilization of NRF2 and reduced expression of its target genes. Interestingly, a significant decrease in the activation of PI3K-Akt pathway has been observed in the SNpc of PD patients[45] and a decline in NRF2 expression has been detected in AD and PD patients with age-dependent cognitive loss[46–48].

Our data point to an important role of astrocytes in the gene expression changes and decreased NRF2 signaling induced by loss of *Park7*. Indeed, reduction of NRF2 in astrocytes has been associated with increased PD pathology[49], while NRF2 overexpression induces cytoprotection and reduction of symptoms[46,48,50,51]. Consistently, *Park7* and *Nfe2l2* knockdowns in male astrocytes, but not in microglia or oligodendrocytes, led to downregulation of *Cyp1b1* and *Cdh1* expression, in keeping with the results obtained in vivo. Moreover, *Cyp1b1* knockdown alone also decreased expression of *Cdh1* and other target genes, linking CYP1B1 enzyme to the enriched processes such as EMT, focal adhesion, and ECM-interaction in astrocytes. Interestingly, an association of CYP1B1 with the regulation of EMT and redox homeostasis in astrocytes has already been reported[52]. While astrocytes are unlikely to undergo classical EMT upon loss of *Park7*, astrogliosis has been proposed to be an EMT-like process involving a subset of EMT-related genes, in particular those linked to ECM and adhesion[53]. Remarkably, ECM and focal adhesion were found among the common PD-associated transcriptome signatures in a recent analysis of midbrain neurons derived from PD patients with many different genetic causes[54]. And finally, DJ-1 has already been associated with alterations in the ECM and promotion of EMT in the context of cancer[55].

Importantly, the top upstream regulator predicted to explain expression changes in the midbrain of *Park7*$^{-/-}$ male mice at the age of 8 months was *17β*-oestradiol. Therefore, the neuroprotective role that *17β*-oestradiol, the main female hormone, plays in the brain, including reduction of ROS levels or activation of antioxidant enzymes[56,57], may lead to the sexual dimorphism observed in the midbrain transcriptomic profiles of *Park7*$^{-/-}$ mice at 8 months of age[12]. This is consistent with the fact that incidence and prevalence of PD are higher in males than in females, and that the severity of the symptoms in males are greater[5,58]. In females, the onset of PD correlates positively with onset of menopause and fertile life span[59]. Shorter fertile period or lower exposure to estrogen during life are associated with PD in females[60,61], while increased endogenous estrogen exposure is associated with reduced severity of motor impairment and later onset of PD[62]. Interestingly, the menstrual cycle, a period in which the levels of estrogen strongly fluctuate, can influence in the severity of symptoms in females with PD[63]. Indeed, low-dose estrogen treatment during 8 weeks in Parkinsonian postmenopausal females with motor fluctuations had a significant decrease in motor disability[64].

Thus, there is an increasing body of evidence for sex-specific differences in the phenotypic presentation of PD that also include specific changes in gene expression[65]. As PD is recognized as a heterogenous disorder, monogenic forms of PD represent prototypes for dissecting subtypes of PD with different pathophysiological mechanisms involved. DJ-1 is a rare form

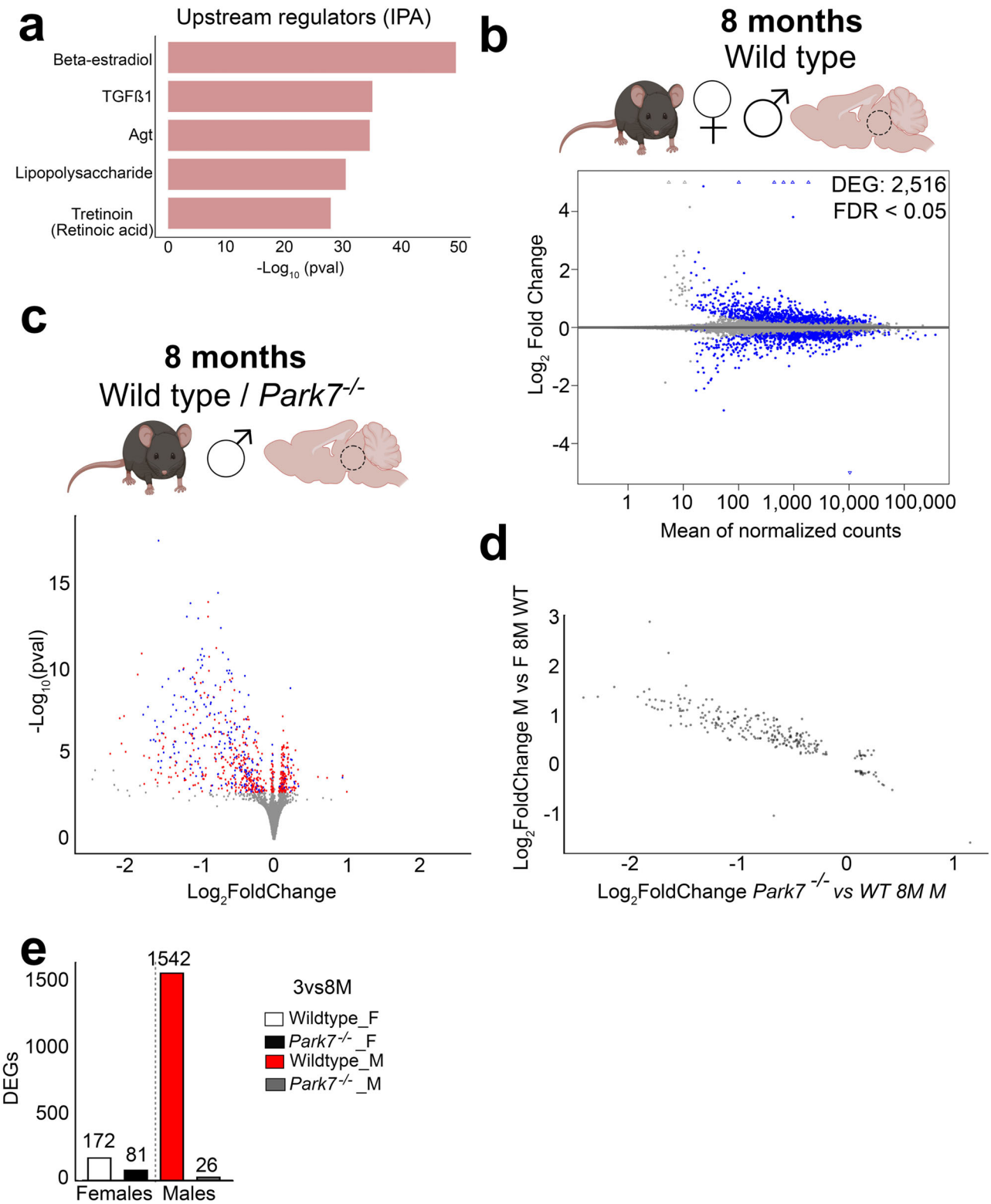

Fig. 4 | *Park7* deletion affects genes with sex-specific expression profile in midbrain. a Top5 Upstream Regulators associated with DEGs from *Park7*$^{-/-}$ male mice and predicted by Ingenuity Pathway Analysis (IPA). The *x*-axis represents the -$\log_{10}$ *p*-value of pathway enrichment. Beta-estradiol is the most enriched regulator while retinoic acid (tretinoin) is fifth most significant. **b** MA plot depicting the 2516 DEGs between wild type male and female midbrain in 8-month-old mice ($n = 4$–8). Each blue dot represents a DEG defined by FDR < 0.05. The x-axis represents the mean of normalized counts and the y-axis the $\log_2$-fold change. **c** Volcano plot depicting the 746 DEGs altered in 8-month-old male mice and their overlap with the 2516 DEGs from the (**b**) ($n = 8$). Each red dot represents a DEG only upon *Park7*-depletion (FDR < 0.05) while each blue dot represents a DEG in both *Park7*-depletion and in comparison between wild type males and females (FDR < 0.05). Hypergeometric *p*-value of the overlap is 0.0069. The *x*-axis represents the $\log_2$-fold change and y-axis the -$\log_{10}$ *p*-value. **d** Correlation plot of the $\log_2$-fold changes of the overlapping genes in the two different comparisons, revealing a negative correlation. The *x*-axis represents the $\log_2$-fold change of the pairwise comparison between *Park7*$^{-/-}$ and wild type 8-month-old male mice. The *y*-axis represents the $\log_2$-fold change of the same gene for pairwise comparison between wild type male and female mice. **e** The number of genes with differential expression during aging from 3 months to 8 months per genotype and sex. Panels (**b**) and (**c**) were created with Biorender.com.

of early onset PD with only few families affected world-wide, so that only limited clinical observations are available. Among these the authors characterized a family with a striking difference in disease expression between the two homozygous mutation carriers[38]: whereas the male carrier presented with a typical early onset PD starting at age 35, the sister was still presenting no motor symptoms at age 42 and was still normal PET Scan results.

Also *all-trans* retinoic acid appeared among the top upstream regulators linked to the gene expression changes in male *Park7*$^{-/-}$ mice. Interestingly, *17β*-oestradiol and *all-trans* retinoic acid, after binding to and activating their receptors (estrogen receptors (ERs) and retinoic acid receptors (RARs), respectively), can alter the transcription of their target genes, many of which are shared, exerting opposing effects through genomic

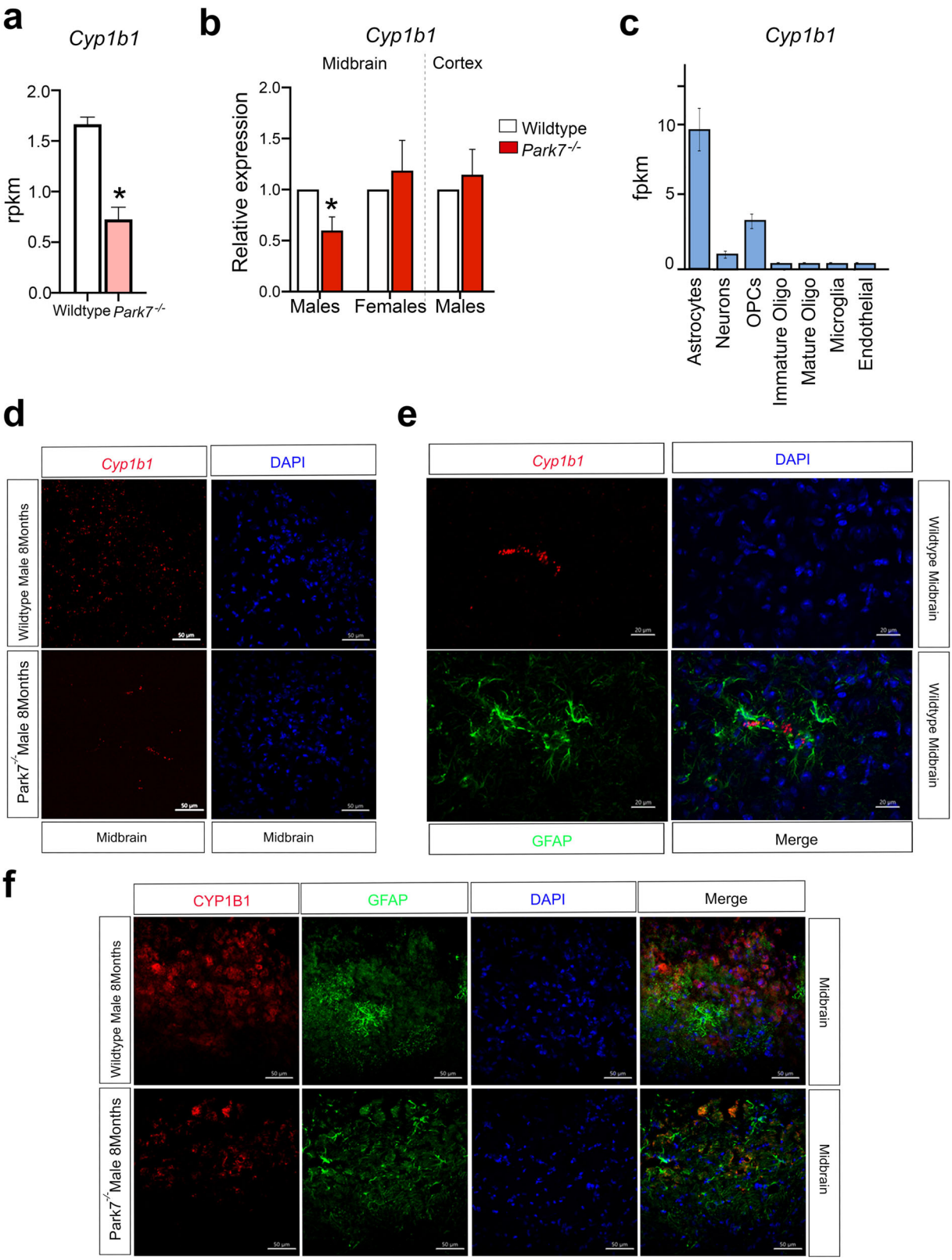

Fig. 5 | Downregulation of Cyp1b1 in the midbrain of male *Park7*$^{-/-}$ mice. **a** Expression levels in RPKM obtained by RNA-seq showing significant downregulation in the expression of *Cyp1b1* in the midbrain of *Park7*$^{-/-}$ male mice at 8 months of age in comparison to wild type mice. *FDR < 0.05. **b** RT-qPCR validation of *Cyp1b1* downregulation in the midbrain of *Park7*$^{-/-}$ male mice at 8 months of age. No downregulation was observed in female ventral midbrain or in male cortex. Values represent mean ± SEM (n = 4–8 mice per group). Statistical significance was tested by unpaired t-test. *p-value < 0.05. **c** Expression levels as fragments per kilobase million (FPKM) of *Cyp1b1* in the different cell populations of the mouse brain obtained from the Brain RNA-seq database from Barres' lab (http://www.brainrnaseq.org/). *Cyp1b1* is mostly expressed in mouse astrocytes. **d** RNAscope validation of *Cyp1b1* downregulation in the midbrain of *Park7*$^{-/-}$ male mice at 8-months of age. *Cyp1b1* mRNA is stained in red, DAPI staining of DNA is in blue. Scale bar indicates 50 µm. Results for female midbrain and male cortex are available in Supplementary Fig. 4. Representative images from analysis of 3 independent mice per genotype are shown. **e** Co-localization of *Cyp1b1* mRNA expression in GFAP-positive astrocytes is illustrated by co-stainings of *Cyp1b1* by RNAscope (red) and GFAP (green) by immunohistochemistry. Scale bar indicates 20 µm. **f** Immunohistochemistry of CYP1B1 (red) and GFAP (green) shows frequent co-localization. DAPI staining of DNA is in blue. Scale bar indicates 50 µm.

antagonism[28]. Some of the known shared target genes between EREs and RARs are related with EMT, ECM, focal adhesion, and antioxidant response[28,66–69]. Therefore it is interesting that CYP1B1 is involved in the metabolism of both *17β*-oestradiol and *all-trans* retinoic acid[70]. Importantly, *Cyp1b1* is among the NRF2-target genes[34], suggesting that NRF2, via transcriptional modulation of *Cyp1b1*, may alter *17β*-oestradiol and *all-trans* retinoic acid levels, with consequences on neuroprotection and regulation of ECM, EMT and focal adhesion, as discussed above.

Finally, another potential upstream regulator we identified was TGF-β. The activity of TGF-β superfamily can be activated by ROS[71]. Therefore, upon an increase in ROS levels in the midbrain, TGF-β signaling could be extraordinarily activated, promoting EMT-related processes. There is a number of reports indicating an interaction between NRF2 signaling and TGF-β pathway via SMAD effector proteins[72–74] Importantly, TGF-β signaling is one of the main pathways regulating GFAP promoter activity and expression[75] and astrocyte-derived TGF-β is involved in the crosstalk between astrocytes and the rest of brain cells, modulating their functions[71]. Therefore, TGF-β signaling is an important regulator of astrocyte formation and function, and its disruption in astrocytes has been associated with pathogenesis of neurological disorders, including PD[76,77].

Importantly, transcriptomic changes in human male iPSC-derived astrocytes with *PARK7* mutation showed overlap regarding the affected pathways with those found in vivo in mice, including EMT as the most enriched pathway for the downregulated genes. This supports the relevance of our findings for understanding PD progression and diagnosis in humans. In addition, upregulated genes were enriched for interferon signaling, similarly to the *Park7*-depleted mouse astrocytes. Interestingly, interferon signaling regulates the activation of PI3-Akt pathway that, as discussed above, may also be altered in the astrocytes of *Park7*$^{-/-}$ mouse midbrain[66].

Taken together, we have described a sex-specific transcriptome signature induced by loss of *Park7* and reveal it to involve dysregulation of EMT, ECM, and focal adhesion associated genes by NRF2 and CYP1B1 in midbrain astrocytes. These results open new avenues for investigation of mechanisms underlying PD progression and its sexual dimorphism.

Material and methods

Animals

Mouse colonies were bred and maintained by the Animal Facility of the University of Luxembourg, on a 12 h light/dark cycle with provided food and water *ad libitum*. All the experiments were conducted following the national guidelines of the animal welfare law in Luxembourg (Règlement grand-ducal adopted on January 11th, 2013), which was approved by the Animal Experimentation Ethics Committee (AEEC) and that follows the European Union guidelines (2010/63/EU).

Park7$^{-/-}$ mice

The *Park7*$^{-/-}$ mice (B6.129P2-Park7Gt (XE726) Byg/Mmucd) used in the present study were already previously characterized[22]. The mice had been backcrossed with C57BL/6 N strain for at least ten generations. The *Park7*$^{-/-}$ and *Park7*$^{+/+}$ mice used in our studies were sex- and age-matched siblings generated from heterozygous *Park7*$^{+/-}$ breeding pairs. The *Park7*$^{-/-}$ and *Park7*$^{+/+}$ mice were bred in-house during three and 8 months, to generate two different study cohorts. For each cohort, both males and females were used. A total of 8 mice (4 male and 4 female) per genotype was used at 3 months of age, while 12 mice (8 male and 4 female) per genotype were used at 8 months of age. Mice were anesthetized with a mixture of ketamine and medetomidine (150 and 1 mg/kg, respectively) and transcardially perfused with PBS (phosphate-buffered saline). After that, brains were extracted and split along the longitudinal fissure in two hemi brains, as described in Karunakaran et al. 2007[78]. Ventral midbrains and cortices of both hemispheres were dissected, snap-frozen in dry ice and stored at -80°C until use.

iPSC-derived astrocytes

The used isogenic iPSC lines C4 and C4mut, harboring the pathogenic c.192 G < C mutation, were previously published[15]. Astrocytes were generated from smNPC via hNSCs as described in Palm et al. 2015[79]. Two days prior to hNSC differentiation, 400 k smNPCs were seeded into one 6-well of a 6-well plate per line. After 2 days, the medium was changed to smNPC medium with 20 ng/ml FGF-2 (Peprotech - 100-18B). After 4 days, the cells were split with Accutase® (Sigma A6964) and the medium was changed to hNSC medium consisting of DMEM/F12 w/o HEPES (Life/Tech – 21331046) supplemented with N2 supplement (Life/Tech – 17502048), B27 supplement with vitamin A (Life Technologies Europe BV/Thermo Fisher Scientific 17504044), GlutaMAX Supplement (Life/Tech – 35050-061), penicillin/streptomycin (Life/Tech – 15140-163), 40 ng/ml EGF (Peprotech - AF-100-15-1mg), 40 ng/ml FGF-2 (Peprotech - 100-18B) and 1.5 ng/ml hLIF (Peprotech - AF-300-05). hNSCs were split with Accutase® when reaching 70-80% of confluence. The astrocytic differentiation medium consisted of the basic cultivation medium DMEM/F12 w/o HEPES (Life/Tech – 21331046) supplemented with 1% penicillin/streptomycin (Life/Tech – 15140-163), 1% GlutaMAX Supplement (Life/Tech – 35050-061) and 1% fetal bovine serum (Life/Tech – 10270-106). 1 million hNSCs per T25 flask were plated 2 days prior to astrocyte differentiation. After 2 days, hNSC medium was changed to astrocyte medium. After 40 days, astrocytes were split to get rid of neurons that are dying during the differentiation and during the process of splitting. After 60 days, astrocytes were considered to be mature and all experiments were conducted around day 60.

Primary cultures and cell isolation

Mixed glial cell cultures were obtained from the brains of 1–3 days old newborn CD1 mice (Charles River, France). After removing meninges and large blood vessels, brains were mechanically dissociated in PBS (phosphate-buffered saline). To keep males and females separated, each individual brain was plated in one T75 flask with culture medium composed of DMEM (Dulbecco's Modified Eagle Medium), 10% FBS (fetal bovine serum) (Life Technologies, 10270-106), 100 U/ml penicillin and 100 µg/ml streptomycin. Furthermore, a small piece of tail (2-3 mm) from each newborn mouse was retained in order to subsequently perform individual sex genotyping (see next section). Mixed glial cell cultures grew at 37°C in a 5% CO2 humidified atmosphere and the medium was changed twice a week.

Two weeks later, once cultures were confluent, cell isolation was performed using a magnetic cell sorting (MACS) method following the manufacturer's instructions (Miltenyi Biotec, The Netherlands). Isolation of specific cell types was performed separately in male and female cultures. An anti-CD11b microbeads antibody (Miltenyi Biotec, 130-049-601) and an anti-O4 microbeads antibody were used to isolate microglia and

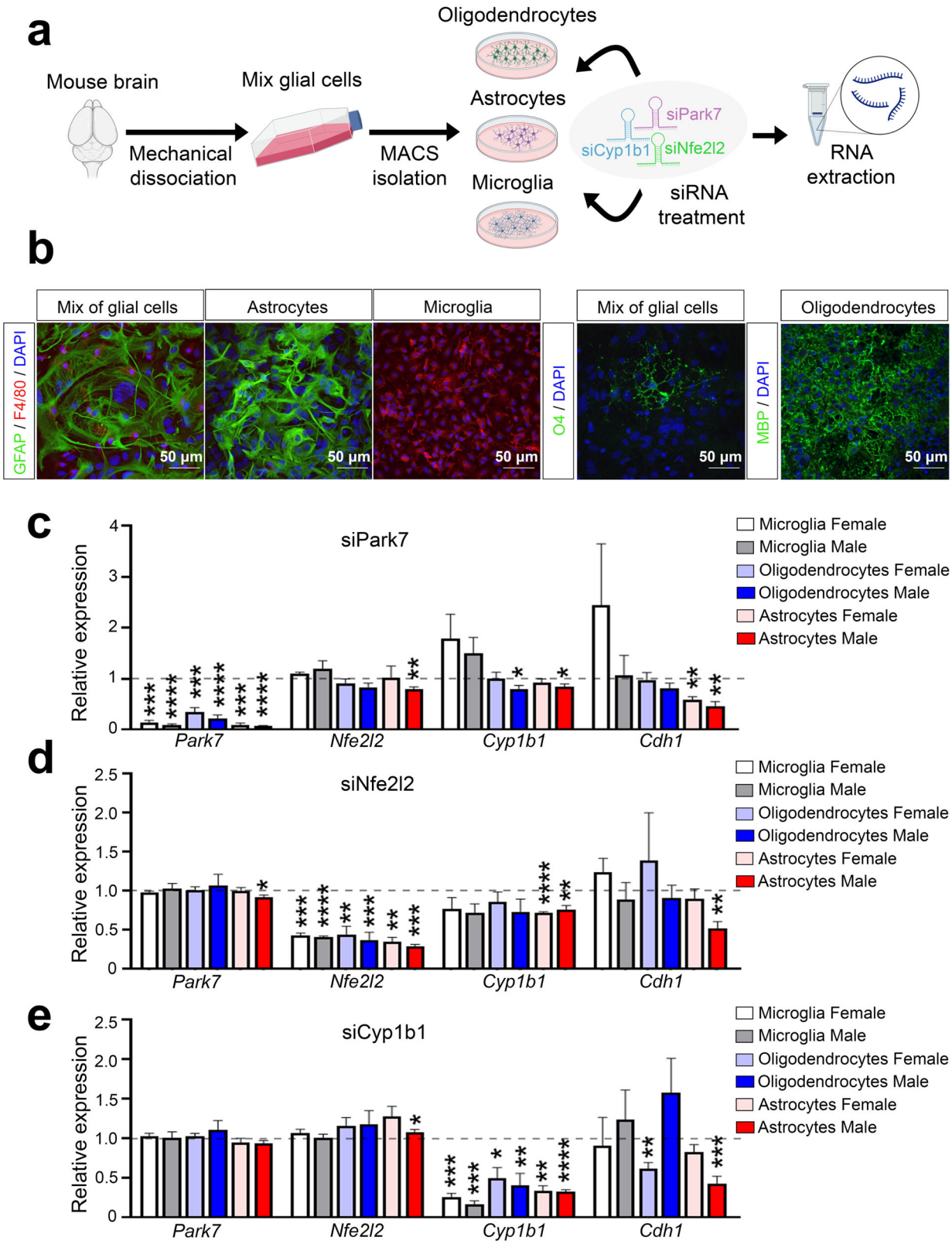

Fig. 6 | Depletion of *Park7*, *Nfe2l2*, and *Cyp1b1* induces downregulation of *Cdh1* in primary male astrocytes but not in microglia or oligodendrocytes. a Schematic diagram of the experimental set-up for glial cell isolation from newborn mice followed by RNAi experiments. Mix of glial cells of each sex were cultured separately after brain removal and mechanical dissociation. From the mixture of glial cells, microglia, astrocytes, and oligodendrocytes were isolated using magnetic cell sorting (MACS) and cultured up to 2 weeks prior to siRNA transfection and RNA extraction 24 h post-transfection. **b** Identity of the isolated cells was confirmed by stainings for GFAP (astrocyte marker, green), F4/80 (microglia marker, red), O4 and MBP (oligodendrocyte markers, green), and DAPI in blue as the nuclear marker. Scale bar indicates 50 µm. **c**–**e** RT-qPCR of gene expression changes upon transfection of siRNAs targeting (**c**) *Park7*, (**d**) *Nfe2l2*, or (**e**) *Cyp1b1*. Expression of *Park7*, *Nfe2l2*, *Cyp1b1* and *Cdh1* was normalized to siScramble per replicate (indicated by dashed line). Values represent mean ± SEM (n = 3-7 mice per group). Statistics were tested by one sample t-test, taking 1 as the theoretical mean. *p-value < 0.05, **p-value < 0.01, ***p-value < 0.001, and ****p-value < 0.0001. Panel (**a**) was created with Biorender.com.

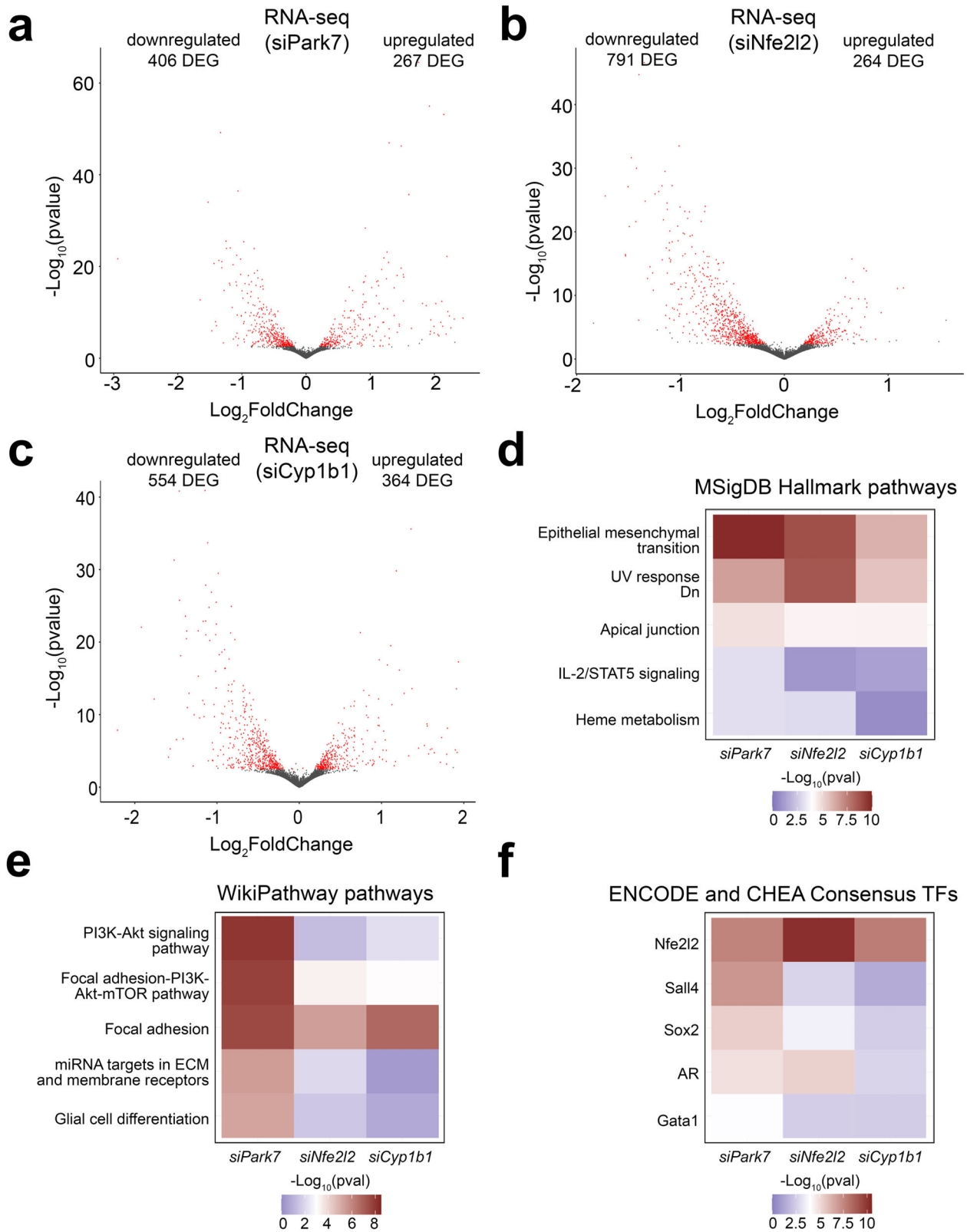

Fig. 7 | Depletion of each *Park7*, *Nfe2l2*, and *Cyp1b1* in primary astrocytes induces downregulation of genes involved in focal adhesion, epithelial-to-mesenchymal transition, and extracellular matrix composition. a–c Volcano plot depicting the DEGs in primary mouse astrocytes upon the knockdown of (**a**) *Park7*, (**b**) *Nfe2l2*, or (**c**) *Cyp1b1* ($n = 3$). Each red dot represents a DEG (FDR < 0.05) and the total number of up- and downregulated DEGs are indicated. The x-axis represents the $\log_2$-fold change and y-axis the $-\log_{10}$ *p*-value. **d–f** Heatmaps showing the differences in pathway enrichments of downregulated DEGs from (**a–c**) using the (**d**) MSigDB Hallmark, (**e**) WikiPathway, and (**f**) ENCODE project and ChEA databases, focusing on the top 5 most enriched pathways or TFs upon *Park7* depletion. The $-\log_{10}$ *p*-values of the enrichments are depicted as color scale.

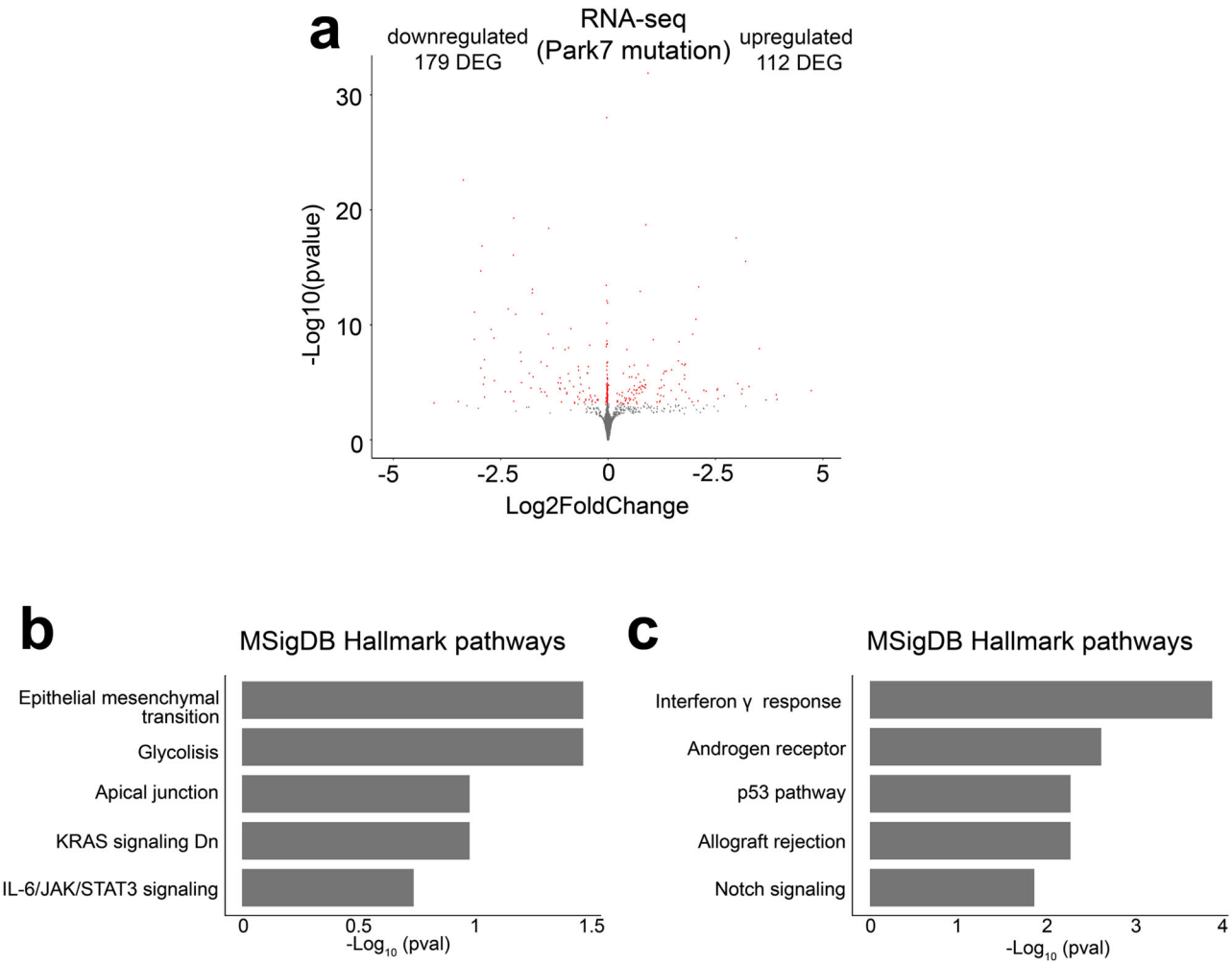

Fig. 8 | DJ-1-dependent transcriptomic changes in human iPSC-derived astrocytes. a Volcano plot depicting the DEGs in male iPSC-derived astrocytes with *PARK7* mutation leading to DJ-1-deficiency when compared to isogenic control cells ($n = 3$). Each red dot represents a DEG (FDR < 0.05) and the total number of up- and downregulated DEGs are indicated. The *x*-axis represents the $\log_2$-fold change and y-axis the $-\log_{10}$ *p*-value. **b**, **c** Pathway enrichment analysis for the 179 downregulated and 112 upregulated DEGs from panel a. The top 5 results from MSigDB Hallmark pathways based on the significance of enrichment are shown for (**b**) downregulated and (**c**) upregulated genes. The x-axis represents the $-\log_{10}$ *p*-value of pathway enrichment.

oligodendrocytes, respectively (positive selection for both). For astrocytes, the negative fraction was kept. To have enough cells, microglia of the same sex were mixed and plated in culture medium composed by mixed glial cell culture-conditioned medium and DMEM (50/50, v/v). $O4^+$ cells of the same sex were also mixed and kept in culture medium composed by MACS Neuro Medium (Miltenyi Biotec, 130-093-570), 2% MACS NeuroBrew-21 (1x) (Miltenyi Biotec, 130-093-566), 0.5 mM L-Glutamine (Lonza, #BE17-605E), 100 U/ml penicillin and 100 µg/ml streptomycin, 10 ng/mL Platelet Derived Growth Factor AA (PDGF-AA) (Miltenyi Biotec, 130-093-978) and 10 ng/mL Fibroblast Growth Factor 2 (FGF-2) (Miltenyi Biotec, 130-105-787), for 14 days with medium change every 2 days. Astrocytes of the same sex are also mixed and kept in culture medium composed of DMEM, 10% FBS, 100 U/ml penicillin and 100 µg/ml streptomycin for 2 weeks, with a second negative selection in between (after 7 days).

Genotyping for sex of primary cultures

Tail fragments (2–3 mm) from each newborn mouse were placed in 1.5 ml eppendorf tubes. After adding 200 µl of Direct PCR Tail (Lysis buffer) (Viagen, 102-T) and 4 µl of proteinase K (Invitrogen, 25530-049), samples were kept for at least 5 h at 55°C with occasional vortexing, to extract the genomic DNA. Afterwards, an equal volume of isopropanol was added, followed by vortexing and centrifugation at 13,000 rpm at 4°C for 10 min. DNA was washed with 200 µl of 70% ethanol and resuspended in 350 µl of DNase/RNase-free water. Afterwards, PCR was performed to amplify the genes *Uba1* and *Ube1y1* on the X and Y chromosome, respectively. For this, we used *Ube* primers that amplify 2 products in males and only the larger product in females[80]. PCR sex genotyping reactions were performed in a final volume of 25 µl with the following reagents and volumes per sample: 12.5 µl KAPA2G Fast HotStart DNA Polymerase (5 U/µL) from the KAPA2G Fast HotStart PCR Kit (Sigma-Aldrich, KK5601), 1 µl of 12.5 µM *Ube* forward primer and 1 µl of 12.5 µM *Ube* reserve primer, 9.5 µl dH2O and 1 µl of purified gDNA; and the following PCR parameters: initial denaturation at 94 °C for 2 min, 35 cycles with 94 °C for 30 s, 57 °C for 30 s, and 72 °C for 30 s, followed by final elongation at 72 °C for 5 min. PCR products were analyzed using agarose electrophoresis together with a DNA ladder (Invitrogen, 10488-058) on 2% agarose gels that contains SYBR safe (Invitrogen, G601802) for the visualization under UV-illumination.

RNA interference in primary cultures

Knockdown of the *Park7*, *Nfe2l2*, and *Cyp1b1* in primary cultures was done using gene-targeted siRNAs. Primary astrocytes were seeded at a density of 4×10^5 cells/well into 12-well plates, while primary microglial cells and oligodendrocytes at a density of 3×10^5 cells/well into 24-well plates. Later, microglia, astrocytes and oligodendrocytes were transfected 2 days, 7 days and 14 days after isolation, respectively. Transfections of 30 nM of siRNAs targeting *Park7*, *Nfe2l2*, *Cyp1b1* or a negative control siRNA (Eurogentec,

Belgium) were done using Lipofectamine RNAiMAX reagent (Life Technologies, Belgium) for 24 h. siRNAs and Lipofectamine RNAiMAX were prepared in DMEM for astrocytes and microglia, while for oligodendrocytes they were prepared in the culture medium (MACS Neuro Medium, 2% MACS NeuroBrew-21 (1x), 0.5 mM L-Glutamine (Lonza), 100 U/ml penicillin and 100 µg/ml streptomycin, 10 ng/mL PDGF-AA and 10 ng/mL FGF-2). After 24 h, RNA from the different cells was extracted.

RNA extraction

For all mouse midbrain samples, RNeasy® Plus Universal Mini Kit (Qiagen, Germany) was used to extract the total RNA. For the different primary cultures, innuPREP RNA Kit (Westburg, The Netherlands) was used to extract the total RNA after 24 h of siRNA transfection. Total RNA was extracted from iPSC derived astrocytes using the Qiagen RNeasy Kit according to manufacturer's protocol.

RT-qPCR

For cDNA synthesis, depending on the sample availability, 100 ng, 300 ng, or 500 ng of total RNA were used. Total RNA was mixed with the following reagents to get a final volume of 40 µl: dNTPs (0.5 mM, ThermoFisher, R0181), oligo dT-primer (2.5 µM), 1 µl RevertAid reverse transcriptase (200 U/µl, ThermoFisher, EP0441), and 1 µl Ribolock RNase inhibitor (40 U/µl, ThermoFisher, EO0381). The reverse transcription was performed at 42 °C for 1 h and stopped by incubating at 70 °C for 10 min. cDNA was diluted 1:5 or 1:3 in DNase/RNase-free water, in the case of using 500 ng or 300 ng of total RNA, respectively.

qPCR reactions were performed using 5 µl of diluted cDNA, 5 µl of a mix containing 2 µM custom designed primers and 10 µl of 1xAbsolute Blue qPCR SYBR green low ROX mix (ThermoFisher, AB4322B), in a final volume of 20 µl per well. Specificity of the primers was verified previously by detecting a single melting point in the melt curve. qPCR parameters were the following: 95 °C for 15 min and then 40 cycles of 95 °C for 15 s, 55 °C for 30 s and 72 °C for 30 s. Gene expression levels were normalized following the $2^{-(\Delta\Delta Ct)}$ method. Briefly, the following formula $(\Delta Ct(_{target\ gene})-\Delta Ct(_{housekeeping\ gene}))_{test\ condition} - (\Delta Ct(_{target\ gene})- \Delta Ct\ (_{housekeeping\ gene}))_{reference\ condition}$ was used to get ΔΔCt. *Rpl13a* was used as the housekeeping gene. To perform statistics, we used GraphPad Prism 9 and to determine the significance, unpaired *t*-test was applied to *Park7*$^{-/-}$ midbrain and cortex samples, and one sample *t*-test was applied in the primary cultures.

RNA-seq

RNA was extracted as described above and its quality was determined by using the Agilent RNA 6000 Nano kit (5064-1511) in an Agilent 2100 Bioanalyzer machine. All samples had a RIN value above 7. mRNA sequencing was performed by the Sequencing Platform of the Luxembourg Centre for Systems Biomedicine (LCSB) of the University of Luxembourg. The TruSeq Stranded mRNA Library Prep kit (Illumina) was used for library preparation. Single-end, stranded sequencing was executed in midbrain samples using an Illumina NextSeq 500 machine with a read length of 75 bp, while paired-end, stranded sequencing was executed in primary astrocytes using a NextSeq2000 machine with a read length of 50 bp.

RNA-seq data analysis

FastQC (v0.11.9) was used to assess the quality control of the raw reads[81]. Reads were trimmed by AdapterRemoval (v2.3.1)[82]. SortMeRNA (v2.1) was used to remove rRNA reads[83], followed by mapping using STAR (v.2.7.4a)[84]. The mouse reference genome used was GRCm38 release 102. Picard tool (v2.10.9)[85] was used to validate the BAM files. After getting the BAM files, featureCounts from the R package Rsubread (v1.28.1)[86] produced the counts of the reads. Using the counts as input, we used R package DESeq2 (v1.20.0)[87] to perform the differential expression analysis and obtain the differentially expressed genes (DEGs). RUVSeq (v1.20.0) was used to remove unwanted variation (batch correction). For primary astrocytes the DEGs were identified using paired analysis due to high variation between between cell isolations. Enrichment analysis for DEGs was conducted with EnrichR[88–90] and Ingenuity Pathway Analysis (IPA)[91]. The distribution of the per-gene dispersion was estimated using DESeq2. The dispersion estimates were obtained after sub-setting the main DESeq2 object with all samples using the different conditions of interest, and then merged into a single table for plotting boxplots and violin plots.

Immunocytochemistry

Mix of glial cells after 14 days in culture, astrocytes after 2 weeks in culture, microglia after 48 h in culture and O4 positive cells (pre-oligodendrocytes and mature oligodendrocytes) after 6 days and 14 days in culture, were seeded on poly-L-lysine coated coverslips into 24-well plates at a density of 3×10^5 cells/well[92] and fixed with 4% PFA for 20 min at room temperature. For permeabilization, 0.3% Triton X-100 in PBS was used for 5 min, followed by 3 washing steps with PBS. Blocking was performed with 3% (w/v) BSA for 30 min at room temperature, followed by an incubation with primary antibodies overnight at 4°C. Mix of glial cells were co-stained using a mouse anti-GFAP antibody (1/300, Cell Signaling, 3670) and a rat anti-F4/80 antibody (1/300, Bio-Rad, MCA497) to check astrocytic and microglial populations. Astrocytes and microglia cultures were also co-stained with the same anti-GFAP and anti-F4/80 antibodies, to check the purity of those cultures and discard any other cell type contamination. Mouse anti-O4 (1/100, R&DSystems, MAB1326) and rat anti-MBP (1/50, Abcam, ab7349) antibodies were also used to check for pre-oligodendrocytes and mature oligodendrocytes respectively. The next morning, cells were incubated with secondary antibodies: Alexa Fluor 488-conjugated donkey anti-mouse (1/1000, ThermoFisher Scientific), Alexa Fluor 488-conjugated donkey anti-rat (1/1000, ThermoFisher Scientific), Alexa Fluor 568-conjugated goat anti-rat (1/1000, ThermoFisher Scientific), or an Alexa Fluor 568-conjugated donkey anti-mouse (1/1000, ThermoFisher Scientific) for 1 h at room temperature. Glass slides with the cells were washed with PBS and mounted with DAPI Fluoromount-G (SouthernBiotech, USA). LSM 510 META inverted confocal microscope at a 40× magnification (Carl Zeiss Micro Imaging, Gottingen, Germany) was used to take the pictures.

RNAscope assay coupled to immunohistochemistry analysis

RNAscope is a multiplex nucleic acid in situ hybridization technology (Advanced Cell Diagnostics, ACD) that enables visualization of different RNA targets at a single cell level. Cryostat sections (20 µm) were prepared from snap frozen tissues (ventral midbrains and cortices) of *Park7*$^{+/+}$ and *Park7*$^{-/-}$ male and female mice, with three independent mice for each genotype. Briefly, frozen slices were immersed in 4% paraformaldehyde for 1 h at 4 °C. After two washing steps in PBS 1X to remove excess fixative, sections were dehydrated in successive ethanol baths (from 50% to 100%) at room temperature (RT). After drying the slides for 5 min, H_2O_2 was applied for 10 min at RT in a HybEZ Humidity Control Tray (ACD). Slices were then submerged twice in ultrapure water before being treated with RNAscope Protease IV for 30 min at RT and washed again twice with ultrapure water. In this work, we used ACD custom probes against mouse cytochrome P450 family 1 subfamily b polypeptide 1 (Mm-Cyp1b1-C1, NM_009994, ACD# 412881-C1), mouse Cadherin 1 (Mm-Cdh1-C2, NM_009864, ACD# 408651-C2) and mouse glutathione S-transferase mu 2 (Mm-Gstm2-O1-C3, NM_008183, ACD# 1332171-C3). Thus, sections were incubated with the corresponding mRNA probes for 2 h at 40°C using the HybEZ Oven (ACD) before being washed twice in 1X washing buffer. Following supplier's protocol, signal was first amplified by a series of incubations using three amplification probes at 40°C for 30 min (Amp1-2) and 15 min (Amp3) and then a series of incubations using respectively RNAscope HRP-C1, HRP-C2 and HRP-C3. For each channel (C1 to C3), dedicated fluorophores (Opal570 and Opal690, 1/1500 dilution, AKOYA Biosciences) were applied on sections for 30 min at 40°C. After each channel amplification, an HRP blocker was added for 15 min at 40°C and two washing steps were performed for 2 min at RT.

In order to visualize astrocytes in our tissue sections, we coupled an immunohistochemistry analysis to our RNAscope procedure. After the last

washing steps previously mentioned, slices were then permeabilized for 30 min at RT with PBS containing 0.5% Triton X100 and blocked with PBS containing 0.5% Triton X100 and 2% Horse serum for 30 min at RT. After two washing steps with PBS, samples were incubated with an anti-GFAP (Guinea-Pig, 1/400 dilution, Synaptic Systems # 173004) for 2 h at RT and washed again twice for 5 min at RT to remove excess primary antibody. Samples were then incubated with Alexa488-conjugated anti-Guinea-Pig (Donkey, 1/400 dilution, Jackson # 706-545-148) for 1 h at RT. Slices were then washed twice with PBS1X for 5 min at RT before being counterstained and mounted. Each tissue section was covered by DAPI for 30 s at RT. After removing DAPI, sections were immediately covered by 1-2 drops of ProLong Gold Antifade Mountant (Life Technologies, # P10144) and a glass coverslip. Slices were dried overnight in the dark and then stored at 4°C. Finally, sections were analysed under an Andor BC43 confocal microscope at a 40-fold magnification.

Immunohistochemistry procedure

We performed immunohistochemistry analysis to detect CYP1B1 expression in mouse brain and kidney tissues. Briefly, frozen slices were immersed in 4% paraformaldehyde for 1 h at 4 °C. After two washing steps in PBS 1X to remove excess fixative, sections were dehydrated in successive ethanol baths (from 50% to 100%) at RT. After drying the slides for 5 min, H_2O_2 was applied for 10 min at RT before being washed in ultrapure water. As previously described in the RNAscope section, slices were permeabilized for 30 min at RT with PBS containing 0.5% Triton X100 and then blocked with PBS containing 0.5% Triton X100 and 2% Horse serum for 30 min at RT. After two washing steps with PBS, sections were incubated with rabbit anti-CYP1B1 antibodies (NovusBio # NBP3-19616, 1/50 dilution) and guinea-pig anti-GFAP antibody (Synaptic Systems # 173004, 1/400 dilution) for 2 h at RT and washed again twice for 5 min at RT to remove excess primary antibodies. Samples were then incubated with Alexa555-conjugated anti-rabbit (Donkey, 1/400 dilution, Life Technologies # A31572) and Alexa488-conjugated anti-Guinea-Pig (Donkey, 1/400 dilution, Jackson # 706-545-148) for 1 h at RT. Slides were then washed twice with PBS1X for 5 min at RT. Each tissue section was then covered by DAPI or DRAQ7 (Cell Signaling, # 7406) for 30 s at RT. After removing DAPI or DRAQ7, sections were immediately covered by 1-2 drops of ProLong Gold Antifade Mountant (Life Technologies, # P10144) and a glass coverslip. Slices were dried overnight in the dark and then stored at 4°C. Sections were analysed under an Andor BC43 confocal microscope at a 40-fold magnification.

Primers

Primer	sequence (5' → 3')
mMCdh1_F	GGCTGGCTGAAAGTGACACA
mMCdh1_R	ACGGCATGAGAATAGAGGATGTACT
mMCrim1_F	GATTCCATTCTGATCGAGGG
mMCrim1_R	AGGCTTTGGACACTAGAATG
mMCyp1b1_F	AGCCAGCAGTGTGATGATATTCTC
mMCyp1b1_R	AGACAGTTCCTCACCGATGCA
mMEphx1_F	CTACAAGCTGATGTCACGGC
mMEphx1_R	AAACCTTTCACGTGGTTGGG
mMGpx8_F	CTGCGTTTAGATTTATTGTTGATTCTTC
mMGpx8_R	GGGTTGACCAGATACTTCCAAAA
mMGstm2_F	GAAAGCACAACCTGTGTGGA
mMGstm2_R	GAGACCCTCTAAGTACTCTGGC
mMNfe2l2_F	TGAAGCTCAGCTCGCATTGA
mMNfe2l2_R	TGGGCGGCGACTTTATTCTT
mMIrs2_F	GCTAAGTCTCATGGATCAGG
mMIrs2_R	GGAAAAGGTCTCTGAACTGT
mMPark7_F	TGCCATCTGTGCAGGTCCTA
mMPark7_R	TGTGACCTTGCATCCAAAACC
mMRpl13a_F	TGGTCCCTGCTGCTCTCA
mMRpl13a_R	CCCCAGGTAAGCAAACTTTCT
mMUbe _F	TGGTCTGGACCCAAACGCTGTCCACA
mMUbe _R	GGCAGCAGCCATCACATAATCCAGATG

siRNAs

siRNA	sequence (5' → 3')
siCyp1b1_F	GCAACUUCGUUCUGGACAA
siCyp1b1_R	UUGUCCAGAACGAAGUUGC
siNfe2l2_F	GACAAGAGCAACUCCAGAA
siNfe2l2_R	UUCUGGAGUUGCUCUUGUC
siPark7_F	CCAGUCUGGAAGAUGCAAA
siPark7_R	UUUGCAUCUUCCAGACUGG

Data availability

The RNA-seq data for this study have been deposited in the European Nucleotide Archive (ENA) at EMBL-EBI under accession number PRJEB59115 (https://www.ebi.ac.uk/ena/browser/view/PRJEB59115).

Code availability

All the RNA-seq analysis code can be found in the following repository: https://github.com/sysbiolux/Helgueta_et_al_2023.

Received: 7 September 2023; Accepted: 9 December 2024;
Published online: 04 January 2025

References

1. Pfeiffer, R. F. Non-motor symptoms in Parkinson's disease. *Parkinsonism Relat. Disord.* **22**, S119–S122 (2016).
2. Lev, N., Roncevich, D., Ickowicz, D., Melamed, E. & Offen, D. Role of DJ-1 in Parkinson's disease. *J. Mol. Neurosci.* **29**, 215–225 (2006).
3. Rodriguez, M., Rodriguez-Sabate, C., Morales, I., Sanchez, A. & Sabate, M. Parkinson's disease as a result of aging. *Aging Cell* **14**, 293–308 (2015).
4. Pringsheim, T., Jette, N., Frolkis, A. & Steeves, T. D. L. The prevalence of Parkinson's disease: a systematic review and meta-analysis. *Mov. Disord.* **29**, 1583–1590 (2014).
5. Moisan, F., Kab, S. & Mohamed, F. Parkinson disease male-to-female ratios increase with age: French nationwide study and meta-analysis. *J. Neurol. Neurosurg. Psychiatry* **87**, 952–7 (2016)
6. Alexander, G. E. Biology of Parkinson's disease: pathogenesis and pathophysiology of a multisystem neurodegenerative disorder. *Dialogues Clin. Neurosci.* **6**, 259 (2004).
7. Haelterman, N. A. et al. A mitocentric view of Parkinson's disease. *Annu. Rev. Neurosci.* **37**, 137 (2014).
8. Schapira, A. H. V. Mitochondrial pathology in Parkinson's disease. *Mt. Sinai J. Med.* **78**, 872–881 (2011).

9. Dauer, W. & Przedborski, S. Parkinson's disease: mechanisms and models. *Neuron* **39**, 889–909 (2003).
10. Heurtaux, T. et al. Normal and pathological NRF2 signalling in the central nervous system. *Antioxidants (Basel)* **11**, 1426 (2022).
11. Xiu, J. W., Hayes, J. D., Henderson, C. J. & Wolf, C. R. Identification of retinoic acid as an inhibitor of transcription factor Nrf2 through activation of retinoic acid receptor alpha. *Proc. Natl Acad. Sci. USA* **104**, 19589–19594 (2007).
12. Smith, K. M. & Dahodwala, N. Sex differences in Parkinson's disease and other movement disorders. *Exp. Neurol.* **259**, 44–56 (2014).
13. Le Saux, M. & Di Paolo, T. Influence of oestrogenic compounds on monoamine transporters in rat striatum. *J. Neuroendocrinol.* **18**, 25–32 (2006).
14. Bonifati, V. et al. Mutations in the DJ-1 gene associated with autosomal recessive early-onset parkinsonism. *Science (1979)* **299**, 256–259 (2003).
15. Boussaad, I. et al. A patient-based model of RNA mis-splicing uncovers treatment targets in Parkinson's disease. *Sci. Transl. Med* **12**, 3960 (2020).
16. Klein, C. & Westenberger, A. Genetics of Parkinson's disease. *Cold Spring Harb Perspect Med.* **2**, a008888 (2012).
17. Clements, C. M., McNally, R. S., Conti, B. J., Mak, T. W. & Ting, J. P. Y. DJ-1, a cancer- and Parkinson's disease-associated protein, stabilizes the antioxidant transcriptional master regulator Nrf2. *Proc. Natl Acad. Sci. USA* **103**, 15091 (2006).
18. Goldberg, M. S. et al. Nigrostriatal dopaminergic deficits and hypokinesia caused by inactivation of the familial Parkinsonism-linked gene DJ-1. *Neuron* **45**, 489–496 (2005).
19. Hauser, D. N., Primiani, C. T., Langston, R. G., Kumaran, R. & Cookson, M. R. The polg mutator phenotype does not cause dopaminergic neurodegeneration in DJ-1-deficient mice. *eNeuro* **2**, ENEURO.0075-14.2015 (2015).
20. Kim, R. H. et al. Hypersensitivity of DJ-1-deficient mice to 1-methyl-4-phenyl-1,2,3,6-tetrahydropyrindine (MPTP) and oxidative stress. *Proc. Natl Acad. Sci. USA* **102**, 5215–5220 (2005).
21. Andres-Mateos, E. et al. DJ-1 gene deletion reveals that DJ-1 is an atypical peroxiredoxin-like peroxidase. *Proc. Natl Acad. Sci. USA* **104**, 14807–14812 (2007).
22. Pham, T. T. et al. DJ-1-deficient mice show less TH-positive neurons in the ventral tegmental area and exhibit non-motoric behavioural impairments. *Genes Brain Behav.* **9**, 305–317 (2010).
23. Rousseaux, M. W. C. et al. Progressive dopaminergic cell loss with unilateral-to-bilateral progression in a genetic model of Parkinson disease. *Proc. Natl Acad. Sci. USA* **109**, 15918–15923 (2012).
24. Kang, Y. & Massagué, J. Epithelial-mesenchymal transitions: twist in development and metastasis. *Cell* **118**, 277–279 (2004).
25. Lachmann, A. et al. ChEA: transcription factor regulation inferred from integrating genome-wide ChIP-X experiments. *Bioinformatics* **26**, 2438–2444 (2010).
26. Kwak, M.-K. et al. Modulation of gene expression by cancer chemopreventive dithiolethiones through the keap1-Nrf2 pathway. *J. Biol. Chem.* **278**, 8135–8145 (2003).
27. McCarthy, M. M. Estradiol and the developing brain. *Physiol. Rev.* **88**, 91–124 (2008).
28. Hua, S., Kittler, R. & White, K. P. Genomic antagonism between retinoic acid and estrogen signaling in breast cancer. *Cell* **137**, 1259–1271 (2009).
29. Gegenhuber, B., Wu, M. V., Bronstein, R. & Tollkuhn, J. Gene regulation by gonadal hormone receptors underlies brain sex differences. *Nature 2022* **606**, 153–159 (2022).
30. Muskhelishvili, L., Thompson, P. A., Kusewitt, D. F., Wang, C. & Kadlubar, F. F. In situ hybridization and imunohistochemical analysis of cytochrome P450 1B1 expression in human normal Tissues. *J. Histochem. Cytochem.* **49**, 229–236 (2001).
31. Roeske, T. C., Scharff, C., Olson, C. R., Nshdejan, A. & Mello, C. V. Long-distance retinoid signaling in the zebra finch brain. *PLoS ONE* **9**, e111722 (2014).
32. Hartz, P., Fehlmann, T., Wagenpfeil, G., Unger, M. M. & Bernhardt, R. A CYPome-wide study reveals new potential players in the pathogenesis of Parkinson's disease. *Front Pharmacol.* **13**, 1094265 (2023).
33. Petkova-Kirova, P. et al. SNPs in cytochrome P450 genes decide on the fate of individuals with genetic predisposition to Parkinson's disease. *Front Pharmacol.* **14**, 1244516 (2023).
34. Shin, S. et al. NRF2 modulates Aryl mydrocarbon receptor signaling: influence on adipogenesis. *Mol. Cell Biol.* **27**, 7188–7197 (2007).
35. Zhang, Y. et al. An RNA-sequencing transcriptome and splicing database ofg lia, neurons, and vascular cells of the cerebral cortex. *J. Neurosci.* **34**, 11929–11947 (2014).
36. Mencke, P. et al. DJ-1 mediates regulation of metabolism and immune response in Parkinsons disease astrocytes and Glioblastoma cells. *bioRxiv 2024.* **10**, 621212 (2024).
37. Kander, M. C., Cui, Y. & Liu, Z. Gender difference in oxidative stress: a new look at the mechanisms for cardiovascular diseases. *J. Cell Mol. Med.* **21**, 1024 (2017).
38. Hering, R. et al. Novel homozygous p.E64D mutation in DJ1 in early onset Parkinson disease (PARK7). *Hum. Mutat.* **24**, 321–329 (2004).
39. Delaidelli, A. et al. α-Synuclein pathology in Parkinson disease activates homeostatic NRF2 anti-oxidant response. *Acta Neuropathol. Commun.* **9**, 105 (2021).
40. Magrinelli, F. et al. Pathophysiology of motor dysfunction in Parkinson's disease as the rationale for drug treatment and rehabilitation. *Parkinsons Dis*. **2016**, 9832839 (2016).
41. Gao, H. et al. DJ-1 protects dopaminergic neurons against rotenone-induced apoptosis by enhancing ERK-dependent mitophagy. *J. Mol. Biol.* **423**, 232–248 (2012).
42. Tsai, C. Y. et al. Antioxidant effects of diallyl trisulfide on high glucose-induced apoptosis are mediated by the PI3K/Akt-dependent activation of Nrf2 in cardiomyocytes. *Int J. Cardiol.* **168**, 1286–1297 (2013).
43. Yang, S. Y., Pyo, M. C., Nam, M. H. & Lee, K. W. ERK/Nrf2 pathway activation by caffeic acid in HepG2 cells alleviates its hepatocellular damage caused by t-butylhydroperoxide-induced oxidative stress. *BMC Complement Alter. Med.* **19**, 1–13 (2019).
44. Choi, M. S. et al. Transnitrosylation from DJ-1 to PTEN attenuates neuronal cell death in Parkinson's disease models. *J. Neurosci.* **34**, 15123–15131 (2014).
45. Luo, S. et al. Akt phosphorylates NQO1 and triggers its degradation, abolishing its antioxidative activities in Parkinson's disease. *J. Neurosci.* **39**, 7291–7305 (2019).
46. Schmidlin, C. J., Dodson, M. B., Madhavan, L. & Zhang, D. D. Redox regulation by NRF2 in aging and disease. *Free Radic. Biol. Med.* **134**, 702–707 (2019).
47. Uddin, M. S. et al. Autophagy and Alzheimer's disease: from molecular mechanisms to therapeutic implications. *Front Aging Neurosci.* **10**, 4 (2018).
48. Dinkova-Kostova, A. T., Kostov, R. V. & Kazantsev, A. G. The role of Nrf2 signaling in counteracting neurodegenerative diseases. *FEBS J.* **285**, 3576–3590 (2018).
49. Anandhan, A. et al. NRF2 loss accentuates Parkinsonian pathology and behavioral dysfunction in human α-synuclein overexpressing mice. *Aging Dis.* **12**, 964–982 (2021).
50. Gan, L., Vargas, M. R., Johnson, D. A. & Johnson, J. A. Astrocyte-specific overexpression of Nrf2 Ddlays motor pathology and synuclein aggregation throughout the CNS in the alpha-synuclein mutant (A53T) mouse model. *J. Neurosci.* **32**, 17775–17787 (2012).
51. Burton, N. C., Kensler, T. W. & Guilarte, T. R. In vivo modulation of the Parkinsonian phenotype by Nrf2. *Neurotoxicology* **27**, 1094–1100 (2006).

52. Palenski, T. L., Sorenson, C. M., Jefcoate, C. R. & Sheibani, N. Lack of Cyp1b1 promotes the proliferative and migratory phenotype of perivascular supporting cells. *Lab. Investig.* **93**, 646–662 (2013).
53. Vivinetto, A. L. et al. Zeb2 is a regulator of astrogliosis and functional recovery after CNS injury. *Cell Rep.* **31**, 107834 (2020).
54. Stern, S. et al. Reduced synaptic activity and dysregulated extracellular matrix pathways in midbrain neurons from Parkinson's disease patients. *NPJ Parkinsons Dis.* **8**, 103 (2022).
55. Jin, F. et al. DJ–1 promotes cell proliferation and tumor metastasis in esophageal squamous cell carcinoma via the Wnt/β–catenin signaling pathway. *Int J. Oncol.* **56**, 1115–1128 (2020).
56. Sawada, H. et al. Estradiol protects mesencephalic dopaminergic neurons from oxidative stress-induced neuronal death. *J. Neurosci. Res.* **54**, 707–719 (1998).
57. Wang, J., Green, P. S. & Simpkins, J. W. Estradiol protects against ATP depletion, mitochondrial membrane potential decline and the generation of reactive oxygen species induced by 3-nitroproprionic acid in SK-N-SH human neuroblastoma cells. *J. Neurochem.* **77**, 804–811 (2001).
58. Hirsch, L., Jette, N., Frolkis, A., Steeves, T. & Pringsheim, T. The incidence of Parkinson's disease: a systematic review and meta-analysis. *Neuroepidemiology* **46**, 292–300 (2016).
59. Lopes-Ramos, C. M. et al. Sex differences in gene expression and regulatory networks across 29 human tissues. *Cell Rep.* **31**, 107795 (2020).
60. Saunders-Pullman, R. et al. Role of endogenous and exogenous hormone exposure on the risk of Parkinson disease. *Annu. Am. Acad. Neurol.* **23**, S23 (2009).
61. Ragonese, P. et al. Risk of Parkinson disease in women: effect of reproductive characteristics. *Neurology* **62**, 2010–2014 (2004).
62. Cereda, E., Barichella, M., Cassani, E., Caccialanza, R. & Pezzoli, G. Reproductive factors and clinical features of Parkinson's disease. *Parkinsonism Relat. Disord.* **19**, 1094–1099 (2013).
63. Roeder, H. J. & Leira, E. C. Effects of the menstrual cycle on neurological disorders. *Curr. Neurol. Neurosci. Rep.* **21**, 1–10 (2021).
64. Tsang, K. L., Ho, S. L. & Lo, S. K. Estrogen improves motor disability in parkinsonian postmenopausal women with motor fluctuations. *Neurology* **54**, 2292–2298 (2000).
65. Tranchevent, L.-C., Halder, R. & Glaab, E. Systems level analysis of sex-dependent gene expression changes in Parkinson's disease. *NPJ Parkinsons Dis.* **9**, 8 (2023).
66. Lurie, R. H. & Platanias, L. C. Mechanisms of type-I- and type-II-interferon-mediated signalling. *Nat. Rev. Immunol. 2005* **5**, 375–386 (2005).
67. Fernández, I., Tiago, D. M., Laizé, V., Leonor Cancela, M. & Gisbert, E. Retinoic acid differentially affects in vitro proliferation, differentiation and mineralization of two fish bone-derived cell lines: different gene expression of nuclear receptors and ECM proteins. *J. Steroid. Biochem. Mol. Biol.* **140**, 34–43 (2014).
68. Cui, J. et al. All-trans retinoic acid inhibits proliferation, migration, invasion and induces differentiation of hepa1-6 cells through reversing EMT in vitro. *Int. J. Oncol.* **48**, 349–357 (2016).
69. Rigiracciolo, D. C. et al. Focal adhesion kinase (FAK) activation by estrogens involves GPER in triple-negative breast cancer cells. *J. Exp. Clin. Cancer Res.* **38**, 58 (2019).
70. Carrera, A. N., Grant, M. K. O. & Zordoky, B. N. CYP1B1 as a therapeutic target in cardio-oncology. *Clin. Sci.* **134**, 2897–2927 (2020).
71. Luo, J. TGF-β as a key modulator of astrocyte reactivity: disease relevance and therapeutic implications. *Biomedicines* **10**, 1206 (2022).
72. Chen, Q. S. et al. Schisandrin B attenuates CCl4-induced liver fibrosis in rats by regulation of NrF2-ARE and TgF-β/smad signaling pathways. *Drug Des. Devel Ther.* **11**, 2179–2191 (2017).
73. Oh, C. J. et al. Dimethylfumarate attenuates renal fibrosis via NF-E2-related factor 2-mediated inhibition of transforming growth factor-β/Smad signaling. *PLoS ONE* **7**, e45870 (2012).
74. Sun, C., Li, S. & Li, D. Sulforaphane mitigates muscle fibrosis in mdx mice via Nrf2-mediated inhibition of TGF-β/Smad signaling. *J. Appl. Physiol.* **120**, 377–390 (2016).
75. Diniz, L. P., Matias, I., Siqueira, M., Stipursky, J. & Gomes, F. C. A. Astrocytes and the TGF-β1 pathway in the healthy and diseased brain: a double-edged sword. *Mol. Neurobiol. 2018* **56**(56), 4653–4679 (2018).
76. Muñoz, M. D., de la Fuente, N. & Sánchez-capelo, A. TGF-β/Smad3 signalling modulates GABA neurotransmission: implications in Parkinson's disease. *Int. J. Mol. Sci. 2020* **21**, 590 (2020).
77. Roussa, E., Von Bohlen Und Halbach, O. & Krieglstein, K. TGF-beta in dopamine neuron development, maintenance and neuroprotection. *Adv. Exp. Med. Biol.* **651**, 81–90 (2009).
78. Karunakaran, S. et al. Activation of apoptosis signal regulating kinase 1 (ASK1) and translocation of death-associated protein, Daxx, in substantia nigra pars compacta in a mouse model of Parkinson's disease: protection by alpha-lipoic acid. *FASEB J.* **21**, 2226–2236 (2007).
79. Palm, T. et al. Rapid and robust generation of long-term self-renewing human neural stem cells with the ability to generate mature astroglia. *Sci. Rep.* **5**, 16321 (2015).
80. Chuma, S. & Nakatsuji, N. Autonomous transition into meiosis of mouse fetal germ cells in vitro and its inhibition by gp130-mediated signaling. *Dev. Biol.* **229**, 468–479 (2001).
81. Andrews, S. *FastQC: a Quality Control Tool for High Throughput Sequence Data.* https://www.bioinformatics.babraham.ac.uk/projects/fastqc/ (2010).
82. Schubert, M., Lindgreen, S. & Orlando, L. AdapterRemoval v2: rapid adapter trimming, identification, and read merging. *BMC Res. Notes* **9**, 88 (2016).
83. Kopylova, E., Noé, L. & Touzet, H. SortMeRNA: fast and accurate filtering of ribosomal RNAs in metatranscriptomic data. *Bioinformatics* **28**, 3211–3217 (2012).
84. Dobin, A. et al. STAR: ultrafast universal RNA-seq aligner. *Bioinformatics* **29**, 15–21 (2013).
85. Adams, M. D. et al. The genome sequence of Drosophila melanogaster. *Science (1979)* **287**, 2185–2195 (2000).
86. Liao, Y., Smyth, G. K. & Shi, W. featureCounts: an efficient general purpose program for assigning sequence reads to genomic features. *Bioinformatics* **30**, 923–930 (2014).
87. Love, M. I., Huber, W. & Anders, S. Moderated estimation of fold change and dispersion for RNA-seq data with DESeq2. *Genome Biol.* **15**, 550 (2014).
88. Chen, E. Y. et al. Enrichr: Interactive and collaborative HTML5 gene list enrichment analysis tool. *BMC Bioinformatics* **14**, 128 (2013).
89. Kuleshov, M. V. et al. Enrichr: a comprehensive gene set enrichment analysis web server 2016 update. *Nucleic Acids Res.* **44**, W90–W97 (2016).
90. Xie, Z. et al. Gene set knowledge discovery with enrichr. *Curr. Protoc.* **1**, e90 (2021).
91. Krämer, A., Green, J., Pollard, J. & Tugendreich, S. Causal analysis approaches in ingenuity pathway analysis. *Bioinformatics* **30**, 523–530 (2014).
92. Hoenen, C. et al. Alpha-synuclein proteins promote pro-inflammatory cascades in microglia: stronger effects of the A53T mutant. *PLoS ONE* **11**, e0162717 (2016).

Acknowledgements

We would like to thank Drs Aurélien Ginolhac and Anthoula Gaigneaux for their support with bioinformatic analysis and and Dr Djalil Coowar (Animal Facility of University of Luxembourg) for help with breeding of experimental

mice. The computational analysis presented in this paper were carried out using the HPC facilities of the University of Luxembourg. SH and AS were supported by the FNR within the PARK-QC DTU (PRIDE 17/12244779/PARK-QC). Pauline Mencke was supported by FNR AFR funding (AFR PhD 12447024). MM would like to thank the Luxembourg National Research Fond (FNR) for the PEARL grant P16/BM/11192868. Work of RK is supported by the Fonds National de Recherche (FNR) Luxembourg within the following projects: National Centre for Excellence in Research on Parkinson's disease (NCER-PD), MotaSYN [12719684], MAMaSyn, MiRisk [C17/BM/11676395]. JO was supported by the Post Doc Grant from the Fondation Pelican de Mie et Pierre Hippert-Faber. LS is supported by the grants from Fondation Pelican de Mie et Pierre Hippert-Faber, Luxembourg Rotary Foundation, and Institute of Advanced Studies of University of Luxembourg.

Author contributions

M.B. and L.S. conceived the project with input from M.M. and T.S., S.H., T.H., A.S., M.B., and L.S. designed the experiments and analysis. S.H., A.S,. P.G., and M.B. prepared mouse tissues. S.H. performed all mouse RNA-seq experiments and most bioinformatic analysis. S.H. and T.H. prepared mouse cell cultures and performed RNAi experiments. TH performed immunostainings and RNAscope experiments. P.M., I.B., and J.O. performed the RNA-seq experiments and bioinformatic analysis of the human iPSC-derived astrocytes. R.H. prepared the libraries and performed the sequencing. Y.G. supported bioinformatic analysis and developed methodology. S.H., T.H., A.S., M.B., M.M., T.S., and .LS. analyzed and interpreted data. R.K., M.M., M.B., and L.S. supervised the project. S.H. and L.S. wrote the manuscript. All authors read and approved the final manuscript.

Competing interests

All authors declare no financial or non-financial competing interests.

Additional information

Supplementary information The online version contains supplementary material available at https://doi.org/10.1038/s41531-024-00851-7.

Correspondence and requests for materials should be addressed to Lasse Sinkkonen.